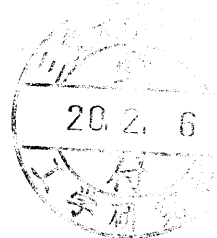


修士論文

乳房 X 線画像における腫瘍陰影を対象とした  
コンピュータ検出支援システムの開発

*Computer-aided Diagnosis Scheme for  
Detection of Masses in Mammograms*



平成 19 年度修了

三重大学大学院 工学研究科

博士前期課程 電気電子工学専攻

水谷洋輔

# Contents

<b>1. Introduction.....</b>	<b>1</b>
1.1. Breast Cancer .....	1
1.2. Mammogram .....	3
1.3. Computer-aided Diagnosis .....	5
1.4. Purpose of This Study .....	6
<b>2. Mammograms Used in This Study.....</b>	<b>8</b>
<b>3. Methods .....</b>	<b>9</b>
3.1. Overall Scheme for Detecting Mass Based on Bilateral Subtraction Technique .....	9
3.2. Segmentation of Breast Regions and Gray-level Transform .....	11
3.3. Enhancement of Nodular Structures .....	15
3.4. Alignment of Right and Left Breast Regions based on Skin Lines .....	17
3.5. Alignment of Right and Left Breast Regions based on Similar ROIs .....	22
3.6. Segmentation of Candidate for Mass .....	24
3.7. Detection of Mass .....	30
<b>4. Results.....</b>	<b>32</b>
<b>5. Discussion.....</b>	<b>36</b>
5.1. Comparison of Detection Performances.....	36
5.2. Undetected masses .....	38
<b>6. Development of Graphical User Interface for     Proposed CAD Scheme.....</b>	<b>41</b>
6.1. Overview of Graphical User Interface.....	41
6.2. Display of Breast Images and the Analysis Result of proposed CAD Scheme .....	42
<b>7. Conclusion.....</b>	<b>43</b>
Acknowledgment .....	43
Appendix: Histogram Specification.....	44
References .....	45

## List of Figures

Figure 1	Number of women who died of breast cancer in Japan .....	2
Figure 2	Medio-Lateral Oblique (MLO) view and Cranio-Caudal (CC) view .....	4
Figure 3	Example of masses with different shape and margin .....	4
Figure 4	Example of mammograms in DDSM .....	8
Figure 5	Schematic diagram of proposed CAD scheme .....	10
Figure 6	Example of the segmentation of breast region and the determination of breast region .....	12
Figure 7	Idea of the histogram specification method .....	13
Figure 8	Example of the histogram specification method .....	14
Figure 9	Example of the enhancement of nodular structures .....	16
Figure 10	Example of the alignment of the nipples .....	18
Figure 11	Method for calculating the distance between right and left skin lines .....	19
Figure 12	Method for searching the best parameters on the angle and the shift .....	20
Figure 13	Right and left breast regions aligned based on skin lines .....	21
Figure 14	Relationship between a ROI on left breast region and the corresponding search region on right breast region.....	23
Figure 15	Examples of subtraction image .....	26
Figure 16	Example of the determination of the threshold value based on Niblack's thresholding technique .....	27
Figure 17	Segmented regions of potential mass based on different .....	28
Figure 18	Example of the segmentation of the area with high pixel values in the small region ....	29
Figure 19	Example of candidates for mass with the circumscribed rectangle .....	30
Figure 20	Example of the result of detecting mass .....	31
Figure 21	Relationships between true-positive fraction and the mean number of false-positives per image when the threshold value of $d$ was varied from 50 to 5,000 .....	33
Figure 22	Relationships between true-positive fraction and the mean number of false-positives per image when the parameter $k$ was varied from 0 to 5 .....	34

<i>Figure 23</i>	<i>FROC curve obtained by varying the parameter <math>k</math> while fixing the threshold value <math>d</math> at 150</i>	35
<i>Figure 24</i>	<i>FROC curves obtained by varying parameter <math>k</math> while fixing the threshold value <math>d</math> at 150</i>	37
<i>Figure 25</i>	<i>Example of original image with undetected mass and the enhanced image for nodular structures</i>	39
<i>Figure 26</i>	<i>Example of right and left breasts which were not aligned correctly because of large difference in skin lines</i>	40
<i>Figure 27</i>	<i>Screenshot of GUI for proposed CAD scheme</i>	41

## ***List of Tables***

<i>Table 1</i>	<i>Three highest true-positive fraction and the mean number of false-positives per image when the threshold value <math>d</math> was 150</i>	35
<i>Table 2</i>	<i>Condition of proposed CAD scheme and other three computerized schemes</i>	37

# ***1. Introduction***

## ***1.1. Breast Cancer***

Breast cancer is one of the major health problems for woman health in developed countries. In the United States, one in eight women has breast cancer during their lives [1]. Therefore, it is estimated that about 40,910 women will die of breast cancer in a year. In Japan, MHLW (Ministry of Health, Labor and Welfare) reported that one in twenty women has breast cancer during their lives. 11,177 women died of breast cancer in 2006 [2]. Breast cancer has the highest disease rate in all the cancers for Japanese women. Figure 1 shows the change in the number of women who died of breast cancer in Japan. It is expected that the number of people who die of breast cancer will increase for some time because the disease rate of breast cancer continues to increase.

It is important to detect breast cancer at early stage before a subjective symptom such as lump appears because they are able to be treated effectively. In Japan, however, medical examination for breast cancer had been carried out by only the palpation for a long time. Only the advanced cancers with lump are able to be recognized in the medical examination based on the palpation. Therefore, mammograms which are able to recognize the smaller cancer began to be used in the medical examination for breast cancer recently.

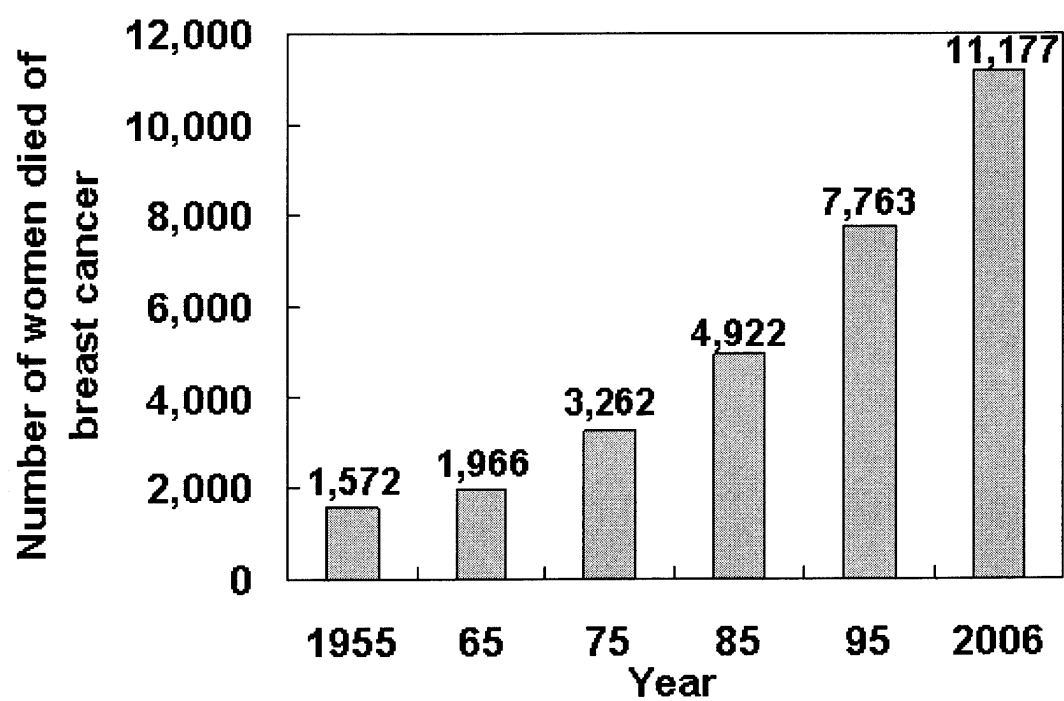


Figure 1 Number of women died of breast cancer in Japan

## 1.2. Mammogram

Mammogram, i.e., an x-ray image for breast, is the most effective method for the early detection of nonpalpable breast cancers. In the United States, therefore, it has been used in the medical examination for breast cancer for about 20 years. In Japan, it was introduced into the medical examination for breast cancer five years ago.

For acquiring mammogram, the breast is squeezed between two plastic plates attached to the mammogram equipment. This squeezing or compression is needed to make it easy to recognize breast lesions by spreading the breast tissue. It also ensures that the image quality becomes sharper despite using a lower radiation dose. A radioactive expose is 0.05 to 0.15 mSv per picture. It has very few effects on the human body. Mammography produces a white image of the breast tissue on a back sheet of film. The breast can be imaged from several angles, i.e., viewpoints. Medio-Lateral Oblique (MLO) view and Cranio-Caudal (CC) view are the most frequently used viewpoints. The viewpoints of MLO view and CC view are shown in Figure 2.

Mass and clustered microcalcifications appear as the important indications which may relate to breast cancer in mammogram. In particular, mass is often very obscure, as shown in Figure 3. It will be noted that the contrast between mass and the surrounding normal breast tissues is very low. Therefore, it is a difficult task for radiologists to detect all masses correctly in mammograms. Actually, Bird *et al.* [3] reported that about 30% of masses are missed by radiologists at mammography in the United States. It is estimated that the miss rate of masses in Japan is higher than that in the United States. In order to reduce the number of missed masses, MHLW recommends the double reading, i.e., the interpretation of mammograms by two radiologists, in the medical examination for breast cancer based on mammography. However, it is difficult to maintain the double reading because there is a shortage problem of radiologists.

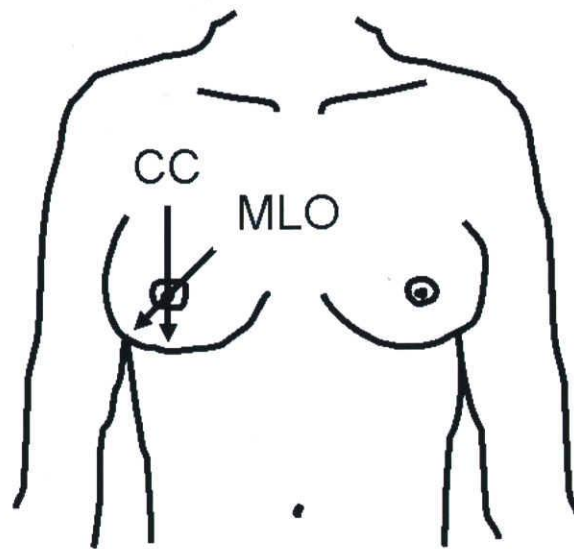
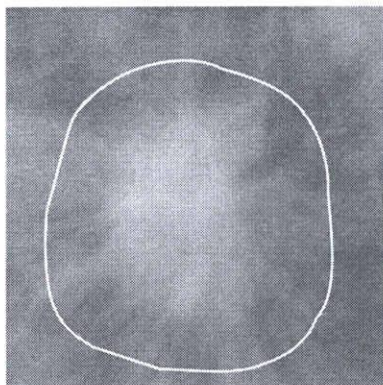
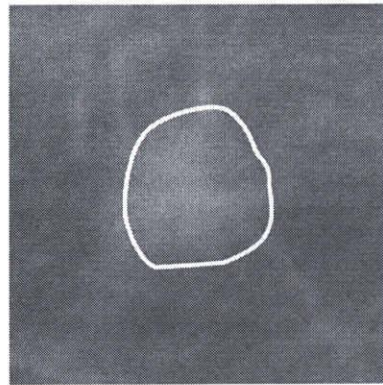


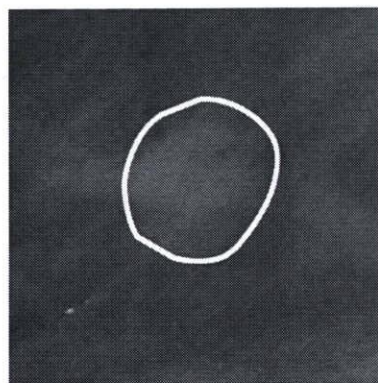
Figure 2 Medio-Lateral Oblique (MLO) view and Cranio-Caudal (CC) view



(a) Irregular shape / spiculated margin



(b) Round shape / ill-defined margin



(c) Oval shape / circumscribed margin

Figure 3 Example of masses with different shape and margin



### ***1.3. Computer-aided Diagnosis***

To reduce the number of missed lesions, Doi *et al.* [4] invented the concept of a computer-aided diagnosis (CAD) scheme for identifying regions of potential lesions in medical images. CAD is defined as a diagnosis made by a radiologist who takes into account the analysis result of CAD scheme as a second opinion. The purpose of CAD is to improve the diagnostic accuracy and the consistency in the radiologists' image interpretation.

On the CAD scheme for mammograms, ImageChecker® was developed by R2 Technology Inc., and it was approved for commercializing from FDA (Food and Drug Administration) for the first time in the world in 1998. After that, in the United States, some CAD schemes have been commercialized by not only R2 Technology Inc. but also GE Healthcare Inc., iCAD Inc., and Kodak Inc.. More than 5,000 commercial CAD schemes have been introduced into medical facilities. About 30% of screening mammograms are screened by radiologists with the CAD scheme in the medical examination for breast cancer based on mammography [5]. In contrast, only CAD scheme of R2 Technology Inc. has been approved for commercializing from MHLW in Japan. The CAD scheme is hardly used in the medical examination for breast cancer based on mammography. This is because the familiarization of mammography is the problem of top priority in Japan where the history of mammography is short.

In 1996, Burhenne *et al.* [6] studied the detection performance of ImageChecker® by using mammograms of 1,083 patients. The detection accuracies of ImageChecker® were 75% for masses and 99% for clustered microcalcifications. In 1999 to 2000, Freer *et al.* [7] evaluated the effect of CAD in interpreting screening mammograms by using data of 12,860 patients. They concluded that the use of CAD can improve the radiologists' detection accuracy of breast cancer at early stage. These studies proved the usefulness of CAD scheme in interpreting screening mammograms. These studies also showed that the detection performance of the CAD scheme for masses was much lower than that for clustered microcalcifications. Therefore, it is necessary to improve the detection performance for mass in CAD scheme in order to reduce effectively the number of missed breast lesions by radiologists.

## ***1.4. Purpose of This Study***

The purpose of this study was to develop a CAD scheme which has high detection performance of masses. Many researchers have developed CAD schemes for detection of masses based on various techniques.

Kupinski *et al.* [8] employed a region growing algorithm based on shape information to detect masses. The partition of region growing was determined by the radial gradient index which means the average proportion of radial gradient. Petrick *et al.* [9] [10] detected masses automatically by applying a Gaussian-Laplacian edge detector to the image in which regions of potential mass were enhanced with the adoptive density-weighted contrast enhancement filter. Karssemeijer *et al.* [11] employed the model based method with gradient information classifying regions of potential mass. Matsubara *et al.* [12] used different gray-level threshold value in the type of breast tissues based on histogram analysis. As the filter for enhancing nodular structure such as mass, Kobatake *et al.* [13], Shimizu *et al.* [14], and Yamamoto [15] developed “Iris filter”, the minimum direction difference filter and “Quoit filter”, respectively. It was difficult for these methods to detect obscure masses which have very low contrast with the surrounding normal tissues.

Experienced radiologists compare normal breast tissues between right and left breasts in order to detect obscure masses. Kopans [16] executed an important observation to compare different mammograms of the same patient: though one breast may be larger than the other, their internal structures were quite symmetric over broad areas. In other words, mass regions appear as the difference in normal breast tissue between right and left breasts. Therefore, other researchers have developed computerized detection schemes based on bilateral subtraction technique which subtracts normal breast tissues between right and left breasts.

In these computerized schemes based on bilateral subtraction techniques, the alignment of right and left breast regions is very important process because it affected directly the detection performance. Yin *et al.* [17] aligned right and left breast regions automatically by rotation and translation based on skin lines and nipple positions. Karssemeijer [18] spaced the pixels of interest point evenly along the breast boundary and the chest wall, and he aligned right and

left breast regions by employing a Thin-Plate Spline which is one of the non-rigid transformation model based on the pixels of interest.

The detection performances of these CAD schemes based on bilateral subtraction technique were relatively higher than those of the methods described in the previous paragraph. This result might indicate that the difference in normal breast tissues between right and left breasts is more useful than the difference between mass and normal tissues in the single breast. In these methods, right and left breast regions were aligned based on only anatomical features such as skin lines and nipple regions. Therefore, internal breast regions weren't always aligned correctly. I thought that it might be possible to detect masses more accurately by using the alignment based on not only skin lines but also internal breast region, i.e., normal breast structures such as blood vessels and mammary glands.

In this paper, I describe a new CAD scheme for detection of masses by aligning right and left breasts accurate. In proposed CAD scheme, right and left breasts are aligned more accurately by two steps of the alignment based on skin lines and the alignment based on normal breast structures. The candidates for mass are then detected by the difference in normal breast tissues between right and left breasts. The detection performance of this CAD scheme is evaluated by using 256 mammograms.

## 2. Mammograms Used in This Study

The database consists of 256 pairs of right and left mammograms which are selected randomly from DDSM (Digital Database for Screening Mammography in the University of South Florida) [19]-[21]. 256 mammograms contain one mass in my database. Thus, the total number of masses is 256. All mammograms are digitized to a pixel size of 0.0435 mm x 0.0435 mm and a 12-bit gray scale, and they are obtained in Portable Gray Map (PGM) format of pseudo 16-bit. The true mass regions determined by an experienced radiologist are provided at the DDSM. Figure 3 shows an example of mammograms with the true mass regions.

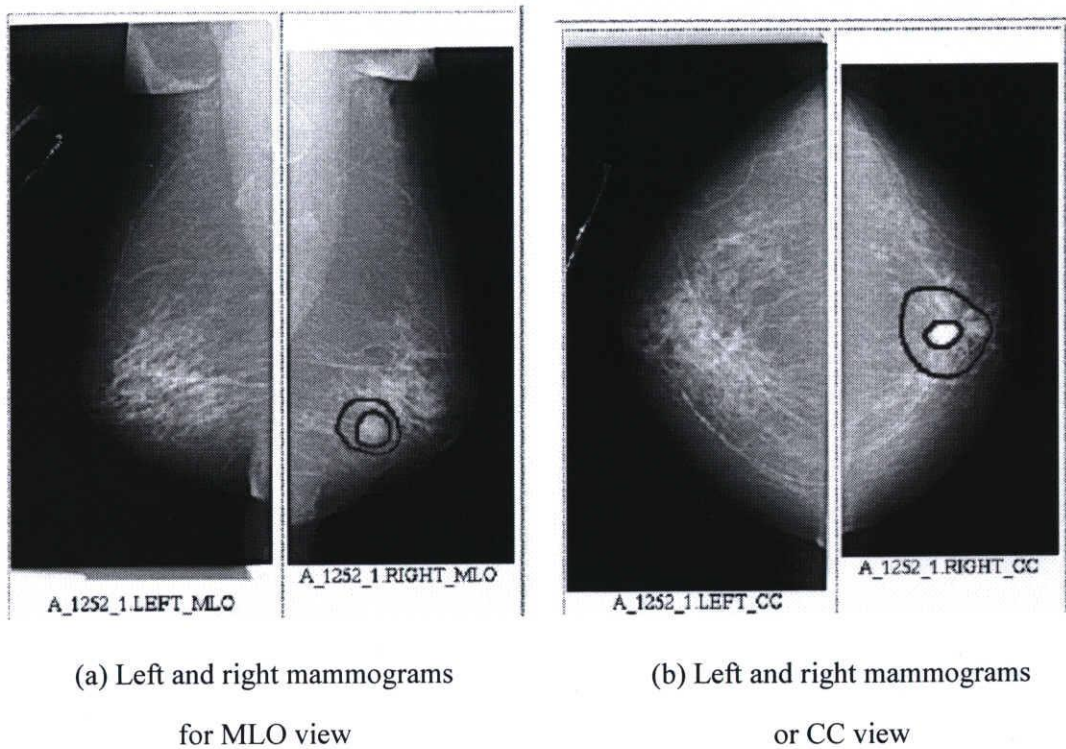


Figure 4 Example of mammograms in DDSM. Each circle indicates the true mass region provided in DDSM.

### ***3. Methods***

In the previous CAD schemes based on bilateral subtraction technique, right and left breast regions were aligned based on only anatomical features such as skin lines and nipple regions. Therefore, internal breast regions were not always aligned correctly. In this paper, I propose a CAD scheme which aligns right and left breast regions in detail by using small region divided into each right and left breast region.

#### ***3.1. Overall Scheme for Detecting Mass Based on Bilateral Subtraction Technique***

Figure 5 shows the schematic diagram of proposed CAD scheme base on bilateral subtraction technique which compares normal breast tissues between right and left breasts. In proposed CAD scheme, breast regions are first segmented from each of right and left mammograms. Gray-levels, i.e. pixel values, are transformed to uniform the histograms based on the pixel values of right and left breast. The nodular structures such as mass are enhanced by the analysis of Hessian matrix. Right and left breast regions are then aligned based on skin lines of right and left breast regions. Each breast region is divided into ROIs (region of interest). In each of ROIs on one breast region, a similar ROI is selected from the neighborhood of the same position in another breast region. The similar ROI is determined by the correlation coefficient based on normal breast structures. Right and left breast regions are also aligned more accurately based on the similar ROIs. The area with high pixel values in the subtraction image between right and left breasts are finally detected as a candidate for mass.

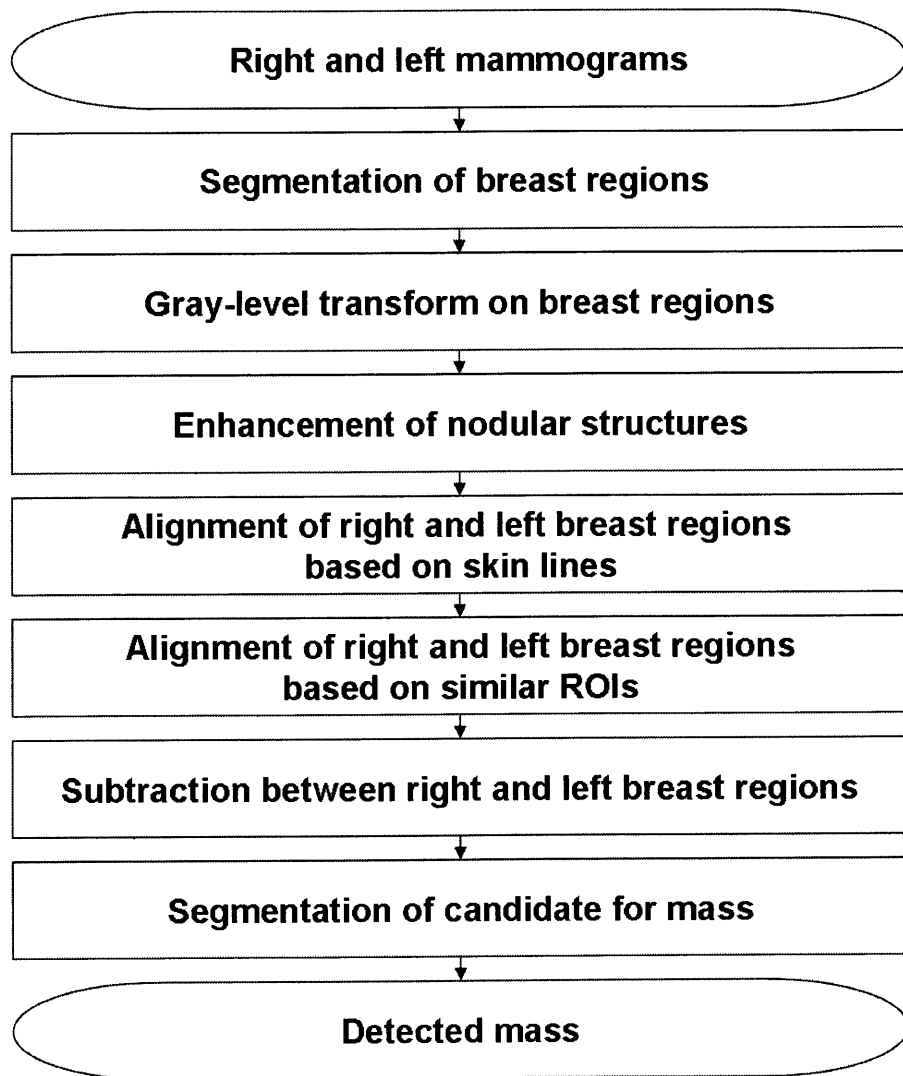


Figure 5 Schematic diagram of proposed CAD scheme

### 3.2. Segmentation of Breast Regions and Gray-level Transform

Each of right and left breast regions is first segmented by a gray-level thresholding technique [22]. 410-pixel value is used empirically as a threshold value. A morphological opening operator [23] is then employed to eliminate non-breast region such as tags of the ID and view point. The structure element for this morphological opening operator is a circle with a radius of 100 pixels. Figure 6 shows an example of the segmentation of breast region and the determination of breast region.

The distributions of pixel values in right and left breasts should be the same in order to compare normal breast tissues between right and left breasts accurately. However, their distributions are often large different. Therefore, the histograms based on the pixel values of right and left breasts are uniformed by a histogram specification method [22]. In this paper, the pixel values on right breast region are transformed to uniform the histograms between right and left breasts. Figure 7 shows the idea of the histogram specification method. The cumulative distribution functions for right breast and for left breast are first obtained from each of the probability functions for right and left breasts. The pixel value for right and left breast and the pixel value for left breast which have the same value of the cumulative distribution functions are defined as the corresponding pixel values. Each pixel value on the right breast is replaced with each corresponding pixel value on the left breast. The transform of histogram specification is expressed by

$$i'_{left} = T^{-1}(C_{right}(i'_{right})) \quad (1)$$

Details are shown in the Appendix. Figure 8 shows an example of the histogram specification method.

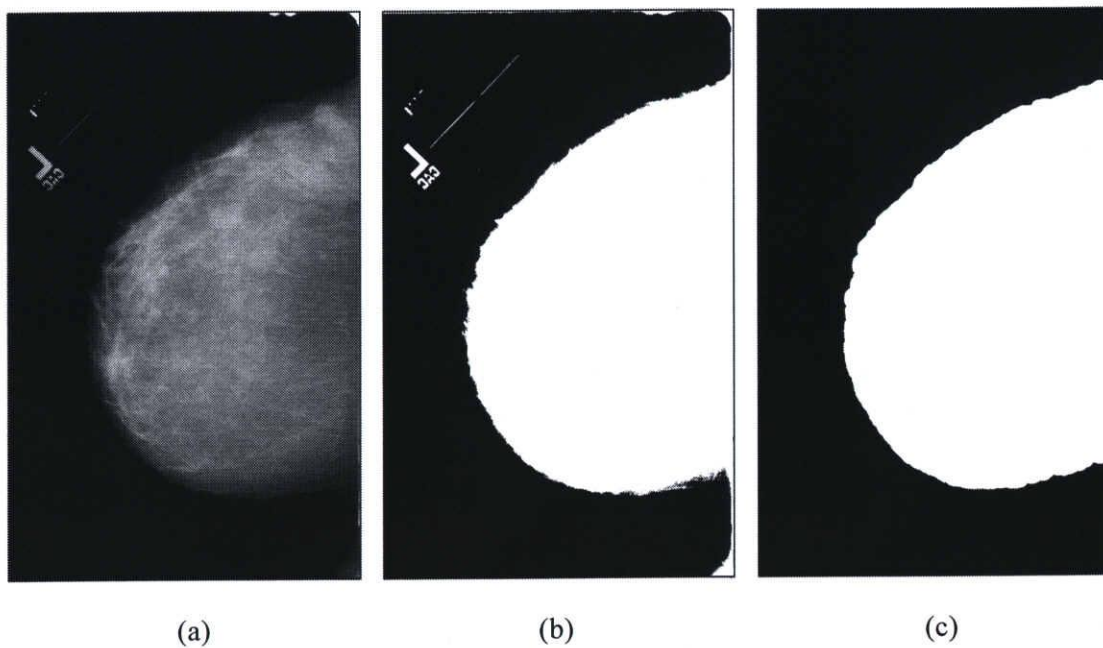


Figure 6 Example of the segmentation of breast region and the determination of breast region: (a) original image, (b) the breast region segmented by a gray-level thresholding technique, (c) the breast region determined by a morphological opening operator.



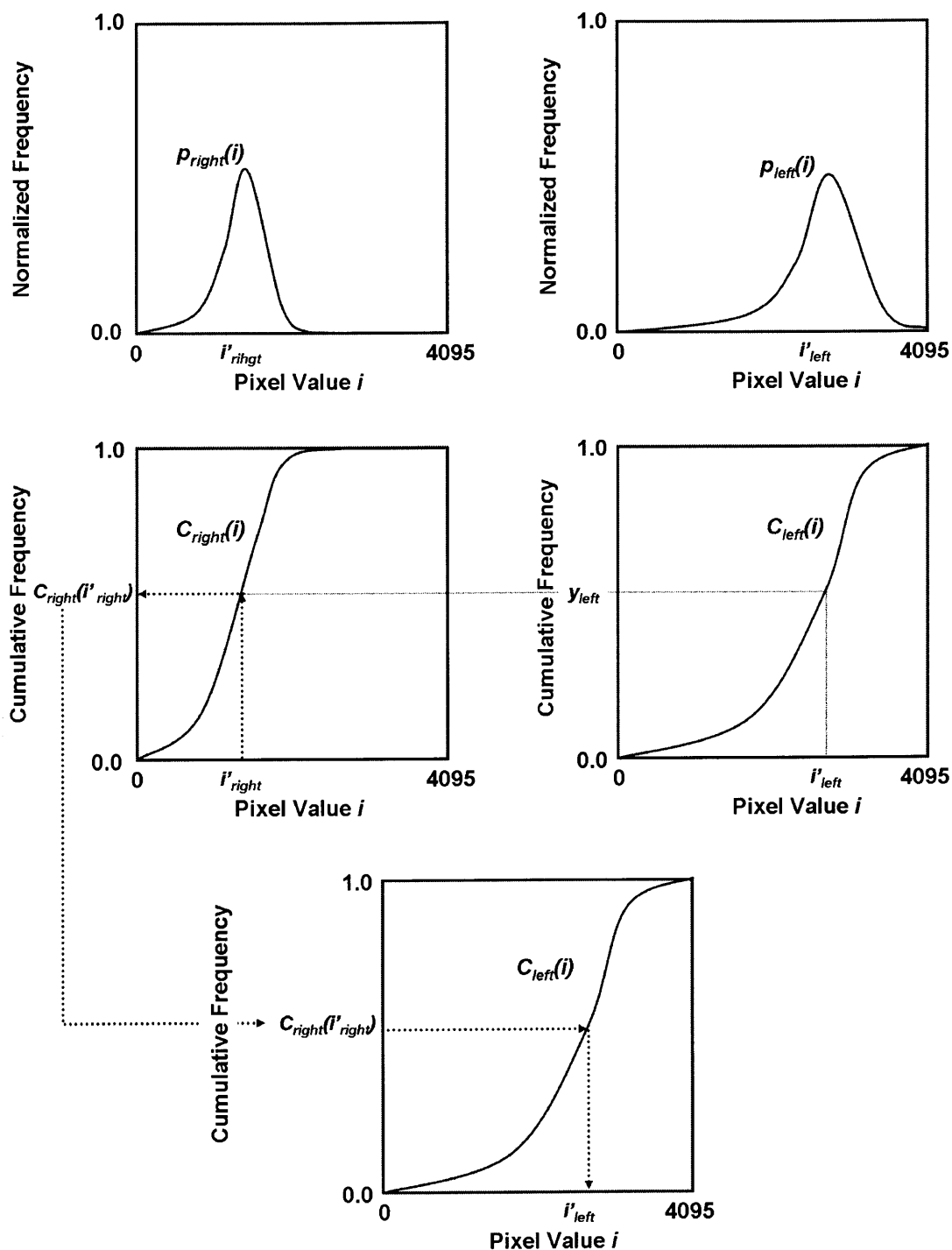


Figure 7 Idea of the histogram specification method: normalized histograms for right and left breasts (top), the corresponding cumulative histograms for right and left breasts (middle), and the cumulative histogram for right breast transformed by histogram specification method. Arrows indicate the pixel value replaced with  $i_{left}$  at pixels which have pixel value  $i_{right}$  in right breast.

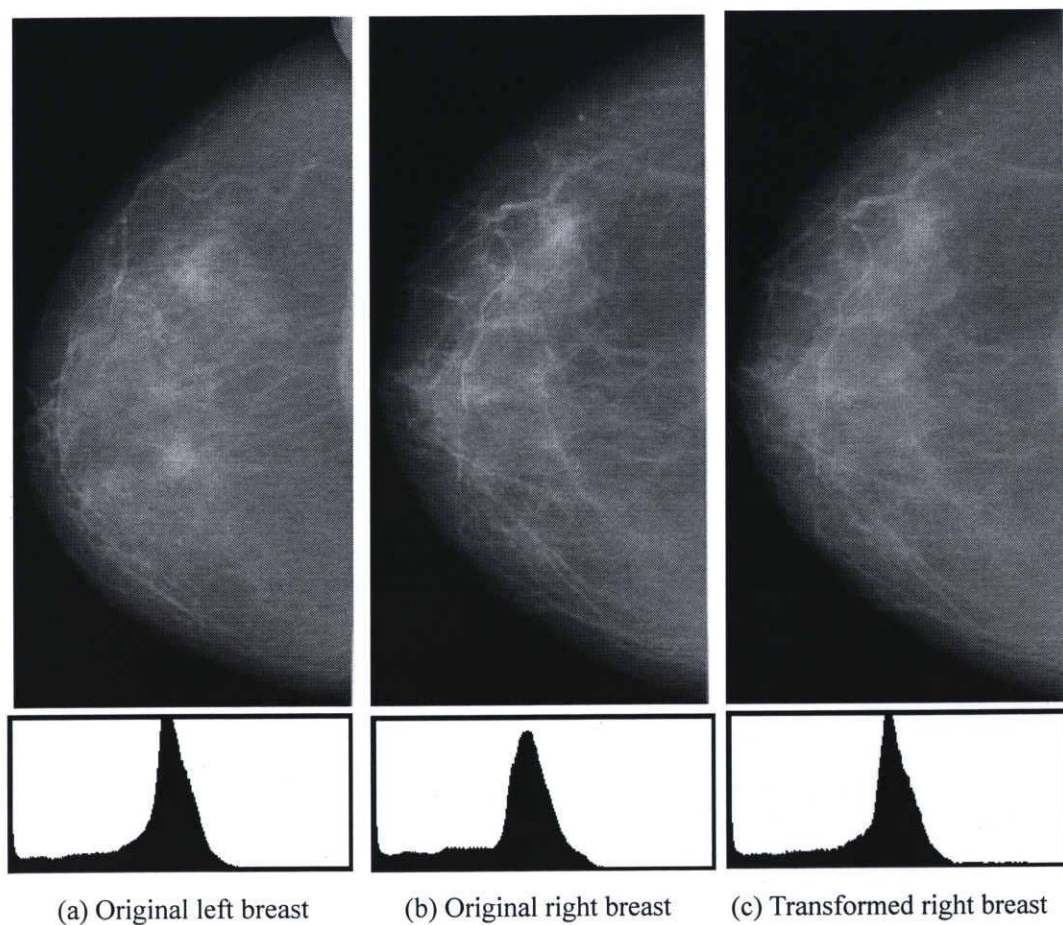


Figure 8 Example of the histogram specification method: (a) original left breast image and its histogram, (b) original right breast image and its histogram, and (c) right breast image transformed by the histogram specification method and its histogram.

### 3.3. Enhancement of Nodular Structures

In the bilateral subtraction technique, it was difficult to detect masses which exist on area where there are many mammary glands with high pixel value. This is because these masses which have very low contrast with surrounding mammary glands appear only as a few differences in normal breast tissue between right and left breasts. Therefore, nodular structures such as mass are enhanced by the eigenvalue of Hessian matrix  $H$  [24]. The each component of Hessian matrix  $H$  is corresponding to the second difference in horizontal direction of the original image, the second difference in vertical direction of the original image, and the first difference in vertical direction followed by the first difference in horizontal direction of original image, respectively. Hessian matrix  $H$  is defined as

$$H = \begin{pmatrix} \frac{\partial^2 f}{\partial x^2} & \frac{\partial^2 f}{\partial x \partial y} \\ \frac{\partial^2 f}{\partial x \partial y} & \frac{\partial^2 f}{\partial y^2} \end{pmatrix} \quad (2)$$

$\frac{\partial^2 f}{\partial x^2}$  : the second difference in horizontal direction

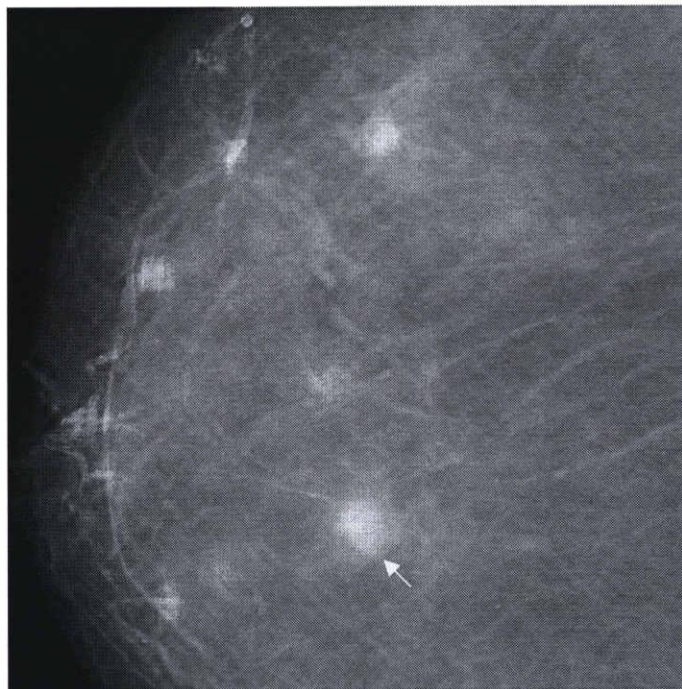
$\frac{\partial^2 f}{\partial y^2}$  : the second difference in vertical direction

$\frac{\partial^2 f}{\partial x \partial y}$  : the first difference in horizontal direction followed by  
the first difference in vertical direction

For detecting microcalcifications which is much smaller than mass, Nakayama *et al.* used from 5-pixel to 13-pixel as the filter sizes of those second different filters [24]. Therefore, it was difficult to detect masses by the same filters. In this paper, 41-pixel is used as the filter size for the second different filter. Figure 9 shows an example of the enhancement of nodular structures.



(a)



(b)

Figure 9 Example of the enhancement of nodular structures: (a) original image, (b) the enhanced image for nodular structures. These images are 2,500 pixels x 2,500 pixels. Each arrow indicates the true mass region.

### 3.4. Alignment of Right and Left Breast Regions based on Skin

#### *Lines*

There are a linear transform and a nonlinear transform as the computerized method for aligning several regions. Affine transform is known as one of the most famous linear transforms. In general, it is defined by a combination of geometric contraction and expansion, translation, rotation, and shear. However, the geometric contraction and expansion, the shear and a nonlinear transform might vary the internal structures of normal breast tissues in breast. Therefore, I considered that it is inappropriate to use their affine parameters and a nonlinear method in proposed CAD scheme based on the difference in normal breast tissues. In this paper, only translation and rotation of affine transform are employed to align right and left breast regions based on skin lines.

In alignment of right and left breast regions, right and left breast regions are first aligned so that right and left nipples exist in left side of each breast region. In other words, one breast region is symmetrically reversed with the vertical axis. Figure 10 shows an example of the alignment of the nipple. Each skin line on right and left breasts is then determined by applying a boundary tracking technique based on four-connectivity [25] to the left side of each segmented breast region. I assumed that the nipples exist on leftmost pixels of skin lines. Therefore, 2,000 of interest points are selected from each of skin lines so that the center of interest points is the leftmost pixel. These interest points are used for determining shift parameter and angle parameter for the affine transform.

These parameters are determined by evaluating the sum of distances between the interest points on left skin line and those on right skin line. A distance  $d(i, j)$  between an interest point  $P_{left}(i)$  on left skin line and the interest point  $P_{right}(j)$  on right skin line is given by

$$d(i, j) = \sqrt{\{x_{left}(i) - x_{right}(j)\}^2 + \{y_{left}(i) - y_{right}(j)\}^2}. \quad (3)$$

Here,  $i, j, x_{left}(i), y_{left}(i), x_{right}(j),$  and  $y_{right}(j)$  are the number of interest point on left skin line, the number of interest point on right skin line, the x coordinate on  $P_{left}(i)$ , the y coordinate on  $P_{left}(i)$ , the x coordinate on  $P_{right}(j)$ , and the y coordinate on  $P_{right}(j)$ , respectively. A distance



$d(i, i)$  between an interest point  $P_{left}(i)$  on left skin line and the corresponding interest point  $P_{right}(i)$  on right skin line is calculated by expression (3). The  $d(i, i-5)$  and the  $d(i, i+5)$  are also calculated in the same way.  $d(i, i-5)$  is the distance between  $P_{left}(i)$  and  $P_{right}(i-5)$  whereas  $d(i, i+5)$  is the distance between  $P_{left}(i)$  and  $P_{right}(i+5)$ . Figure 10 shows the method to calculate the distance between right and left skin lines. The distance  $d(i)$  is defined as the minimum value among  $d(i, i)$ ,  $d(i, i-5)$ , and  $d(i, i+5)$ . The sum of distances  $D$  was determined by.

$$D = \sum_{i=1}^{2000} \min\{d(i, i-5), d(i, i), d(i, i+5)\}. \quad (4)$$

The best parameters for the angle and the shift are searched by rotating angle from  $\pm 10$  degrees at intervals of 0.5 degrees and by shifting in the directions of x-axis (plus and minus quarter of the width of the breast region) and y-axis (plus and minus quarter of the height of the breast region) by one pixel. Figure 11 shows the method for searching the best parameters on the angle and the shift. The angle and the shift are defined as the best parameters when the sum of distances  $D$  of interest points is the minimum value. Figure 12 shows right and left breast regions aligned based on skin lines.

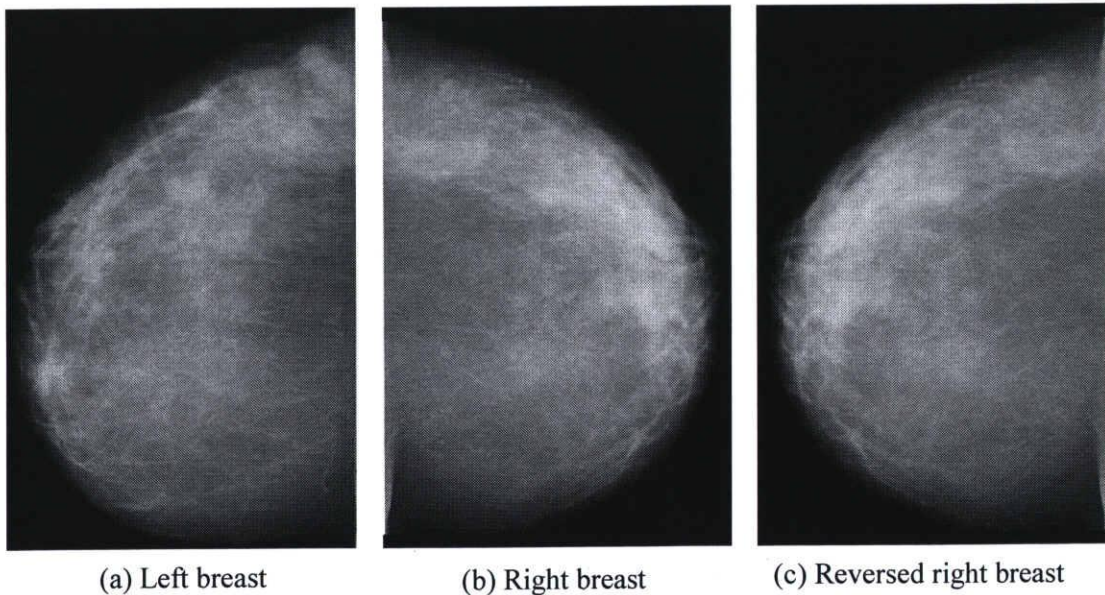


Figure 10 Example of the alignment of the nipples

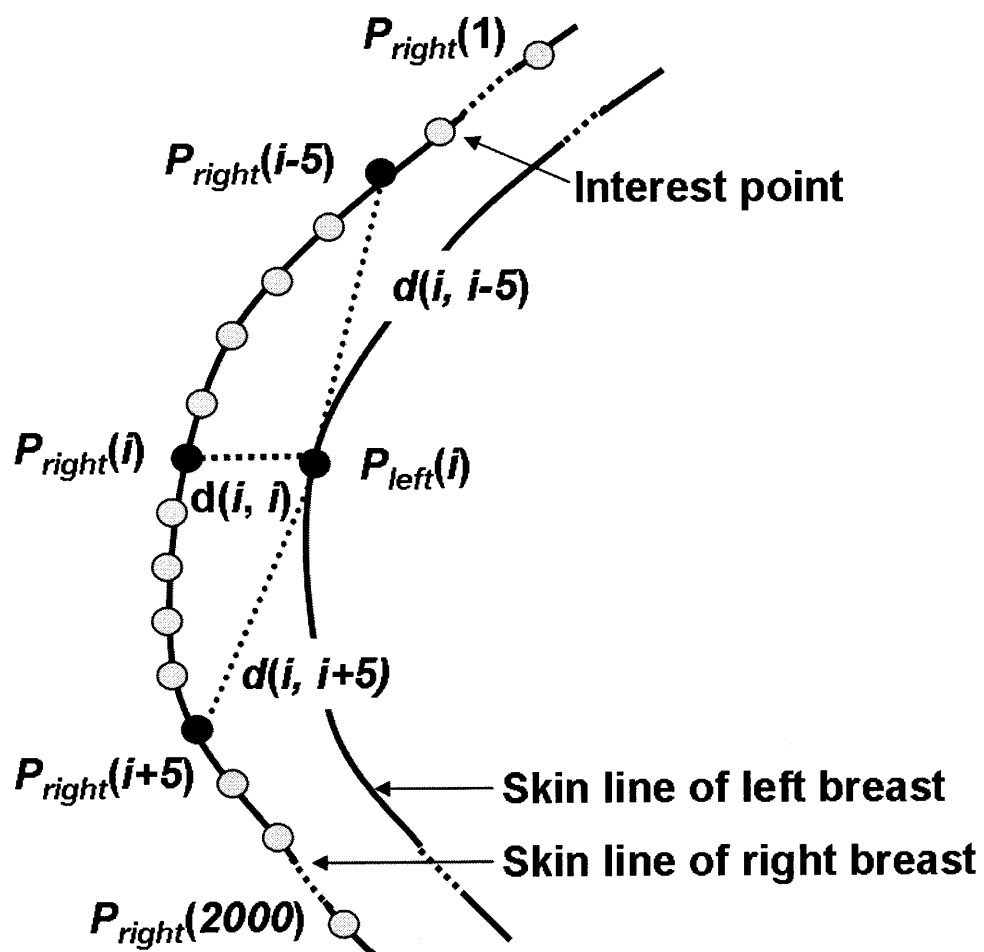


Figure 11 Method for calculating the distance between right and left skin lines

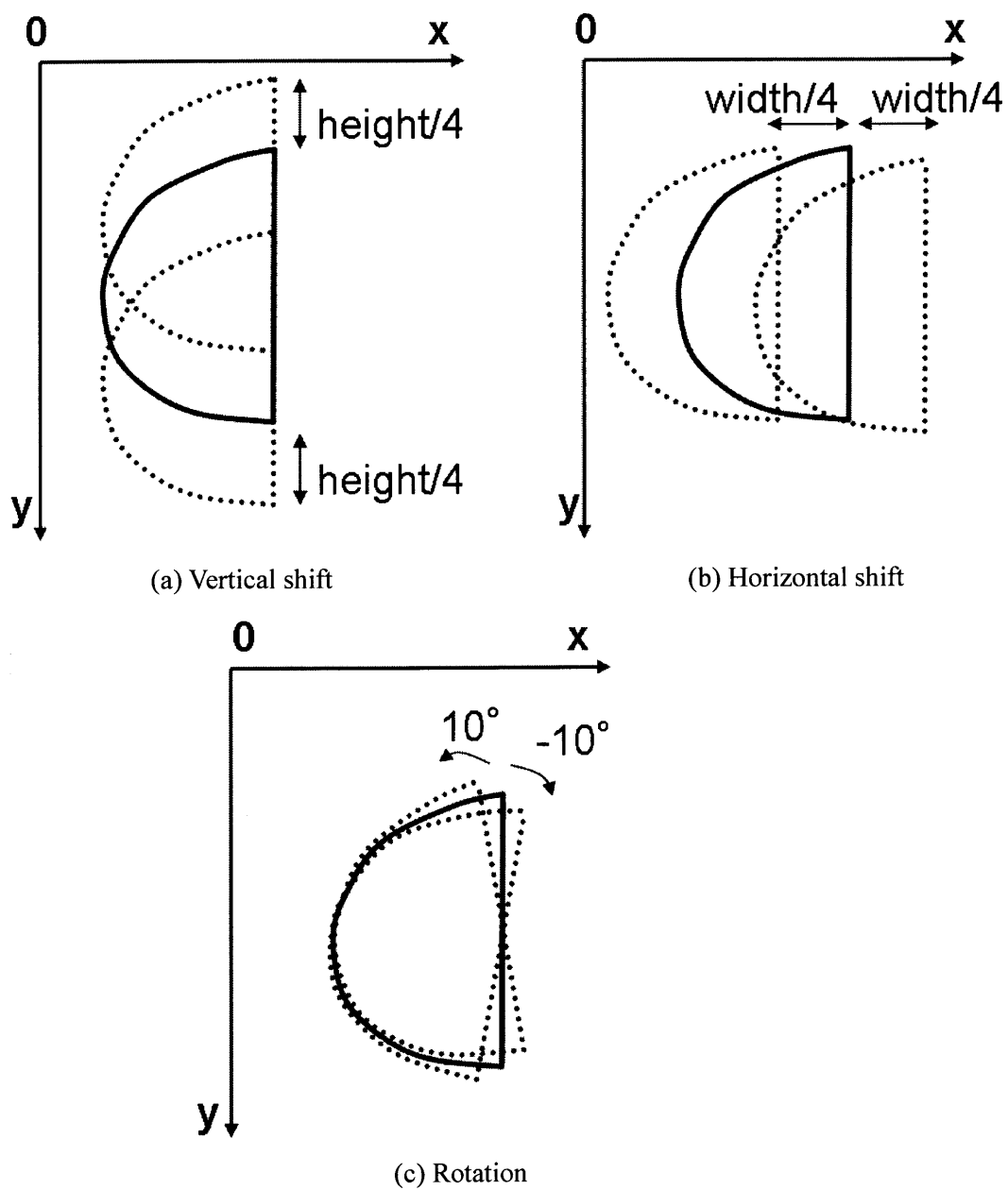
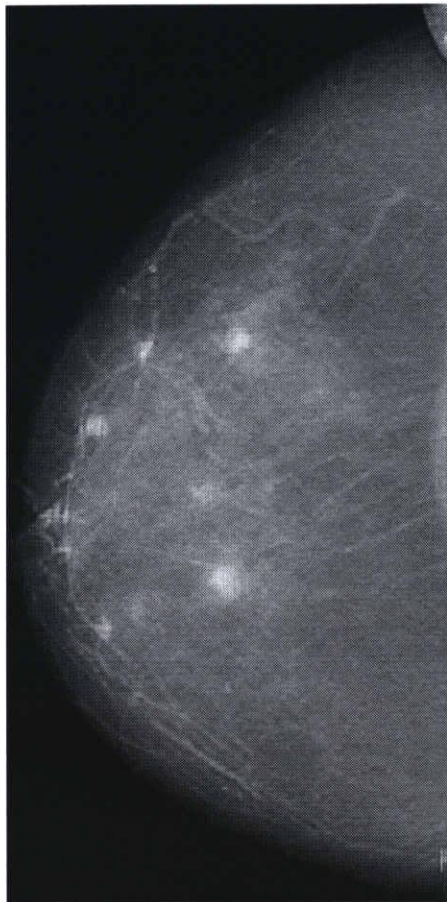


Figure 12 Method for searching the best parameters on the angle and the shift.





(a) Left breast region



(b) Right breast region

Figure 13 Right and left breast regions aligned based on skin lines. The right breast region was translated and rotated by the best parameters for the angle (-3.0 degrees), the horizontal shift (-21 pixels), and the vertical shift (203 pixels).

### 3.5. Alignment of Right and Left Breast Regions based on

#### *Similar ROIs*

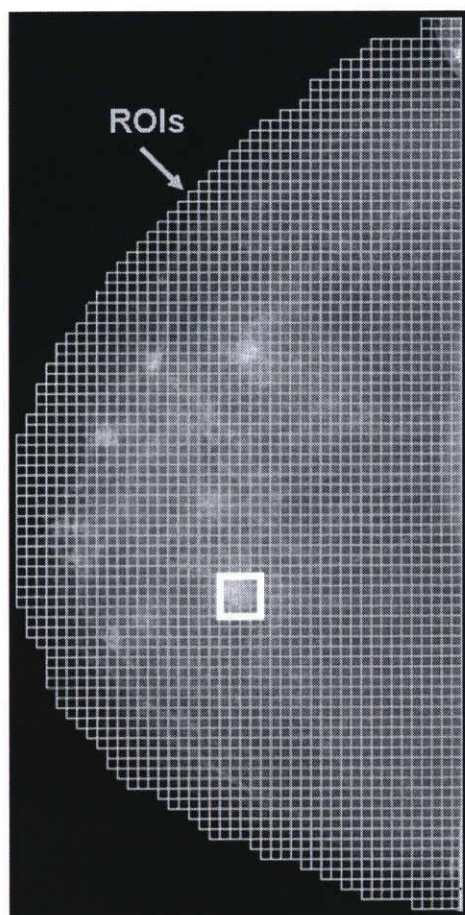
To align right and left breast regions more accurately, right and left breast regions are again aligned by using normal breast structures such as blood vessels and mammary glands. Each of right and left breast regions is first divided into ROIs at intervals of quarter of ROI size (approximately 2.5 mm) so that one ROI would overlap with the adjacent ROIs. The size of each ROI is 230 pixels x 230 pixels (approximately 10 mm x 10 mm). Search regions of 460 pixels x 460 pixels (approximately 20 mm x 20 mm) are then set on right breast region at every position corresponding to the center of each ROI on left breast region. Figure 14 shows the relationship between a ROI on left breast region and the corresponding search region. The correlation coefficients between the ROI on left breast region and each ROI in search region are calculated by

$$r = \frac{\sum \sum \left[ \{f(x, y) - \overline{f(x, y)}\} \cdot \{g(x, y) - \overline{g(x, y)}\} \right]}{\sqrt{\sum \sum \{f(x, y) - \overline{f(x, y)}\}^2} \cdot \sqrt{\sum \sum \{g(x, y) - \overline{g(x, y)}\}^2}} \quad (5)$$

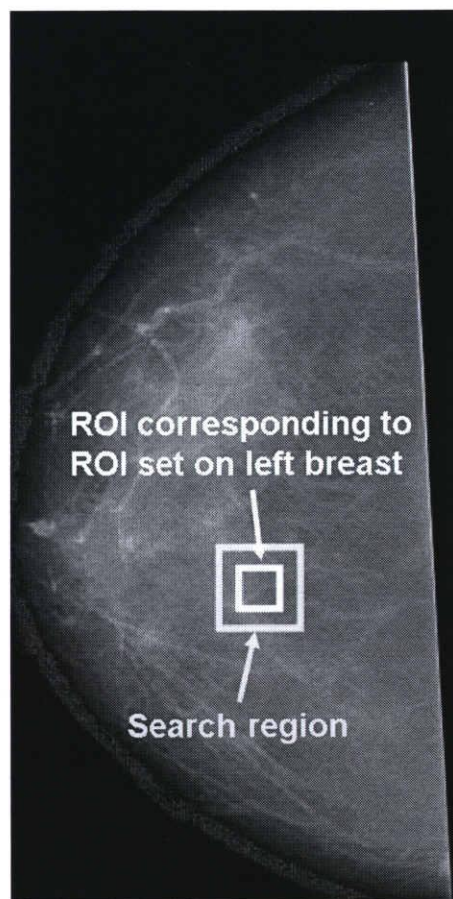
$f(x, y)$  : the pixel value on the position (x,y) of left breast image

$g(x, y)$  : the pixel value on the position (x, y) of right breast image

The ROI with the maximum correlation coefficient in search region is determined as the similar ROI. This procedure is repeated at every ROI on left breast region. Right and left breast regions are finally aligned by the ROI unit based on similar ROI.



(a) Left breast region



(b) Right breast region

Figure 14 Relationship between a ROI on left breast region and the corresponding search region on right breast region

### 3.6. Segmentation of Candidate for Mass

A subtraction image is obtained between right and left breasts aligned by not only skin lines but also normal breast structures. Regions of potential mass will have high pixel values in a subtraction image because normal tissues tend to resemble between right and left breast. Figure 15 shows an example of the subtraction images with masses. In this paper, Niblack's thresholding technique [26] is employed for segmentation of regions of potential mass. Niblack's thresholding technique calculates the mean value and the standard deviation of pixel values in a small region, and determines the threshold value for the center pixel of the small region. The threshold value  $T(x, y)$  at pixel  $(x, y)$  is given as

$$T(x, y) = m(x, y) + k \cdot s(x, y) \quad (6)$$

Here,  $m(x, y)$  and  $s(x, y)$  are the mean value and the standard deviation in the small region centered on the pixel  $(x, y)$ , respectively. If the size of small region is smaller than that of masses included in my database, mass might be divided into several regions by Niblack's thresholding technique. The size of small region has to be large enough to include both of mass region and background region. A 1,380 pixels x 1,380 pixels (approximately 60 mm x 60 mm) is chosen as the size of the small region because the diameters of target mass were determined as smaller than 1,150 pixels (approximately 50 mm).  $k$  is a constant parameter. A threshold value is able to be changed by adjusting  $k$ . When  $k$  is zero, it means that the mean value of the pixel values in small region was used as the threshold value. Figure 16 shows an example of the determination on the threshold value. Figure 17 also shows the segmented region of potential mass based on different  $k$ .

In addition, it is necessary to analyze about whether each of segmented pixel was included in the region of potential mass. This is because Niblack's thresholding technique tends to segment many noises in the small region which has low pixel values. In the analysis of the segmented pixel, the area with high pixel values included in the small region is first segmented by using the threshold value for segmented pixel. Figure 18 shows an example of the segmentation of the area with high pixel values in the small region. The mean values of pixel values in each of white area and black area are then calculated in the small region. If the

difference in these mean values is large, the segmented pixel is considered to be included in the region of potential mass. The region connecting the pixels which is considered to be included in the region of potential mass is defined as a candidate for mass.

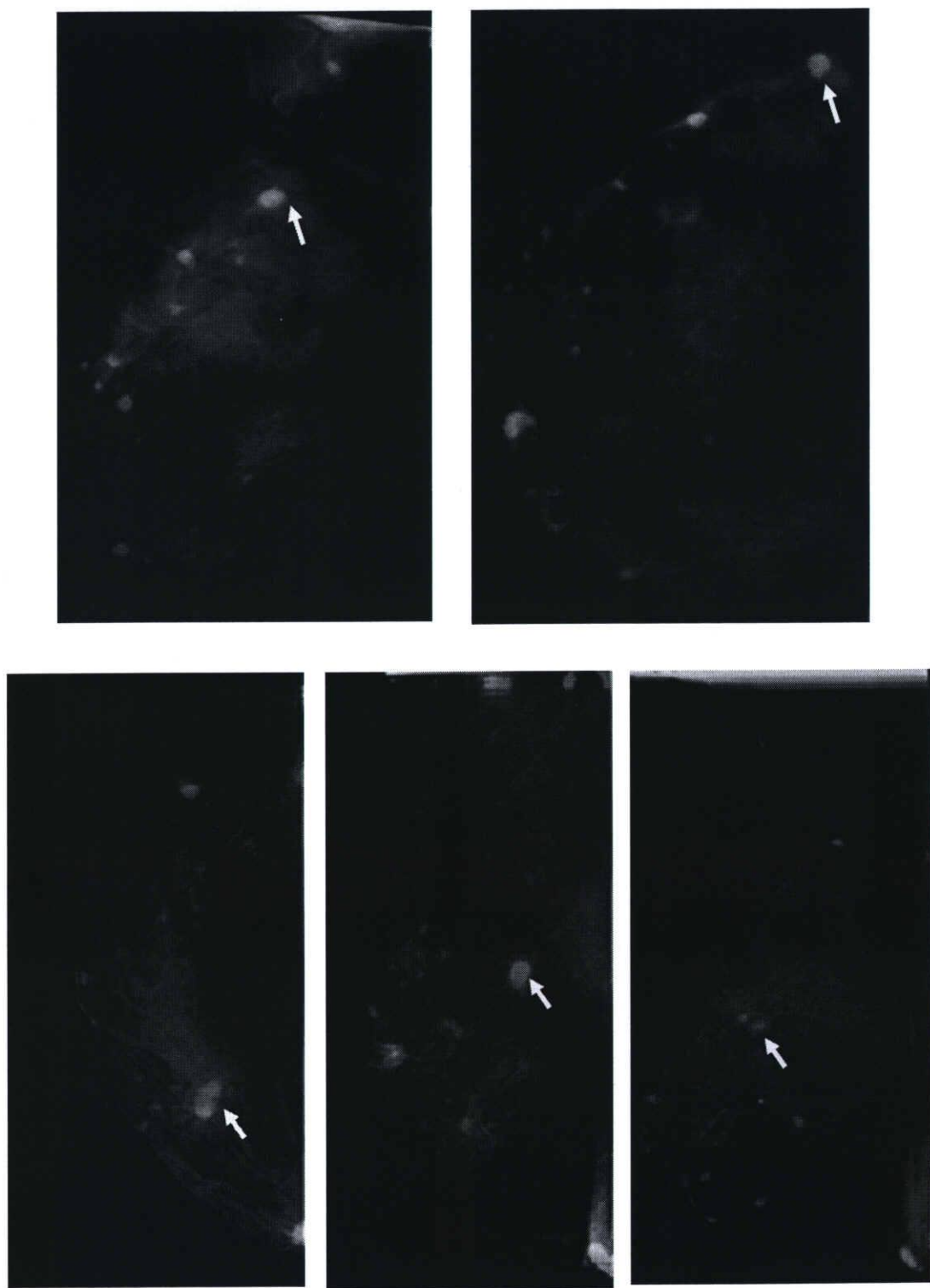
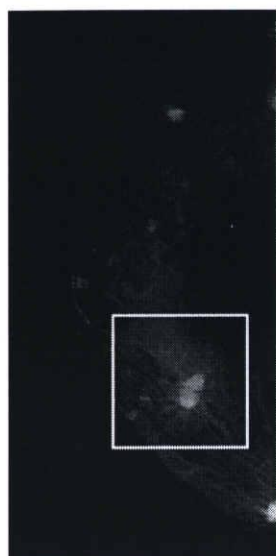


Figure 15 Examples of subtraction images. Each arrow indicates the true mass region.

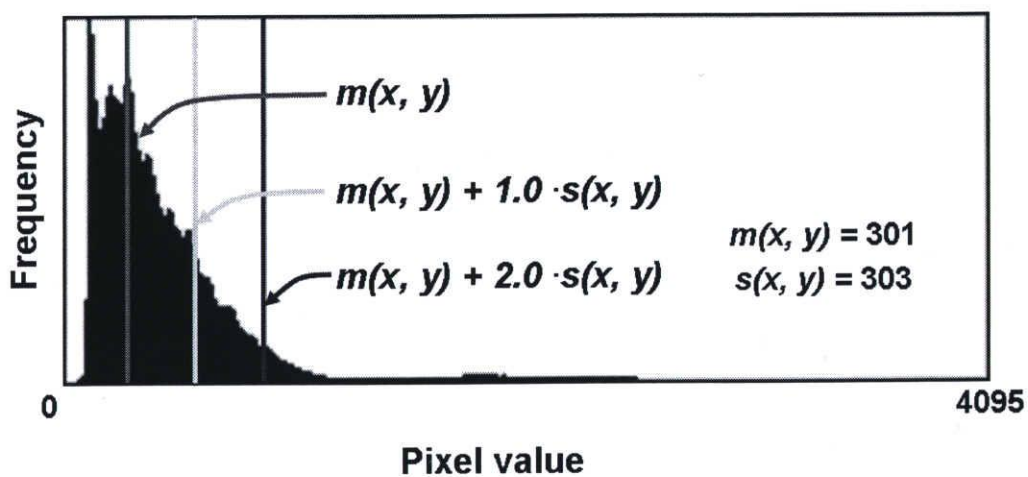




(a) Subtraction image with a small region



(b) Subtraction image in the small region



(c) Histogram for the small region (b) and threshold value in different  $k$

Figure 16 Example of the determination of the threshold value based on Niblack's thresholding technique.

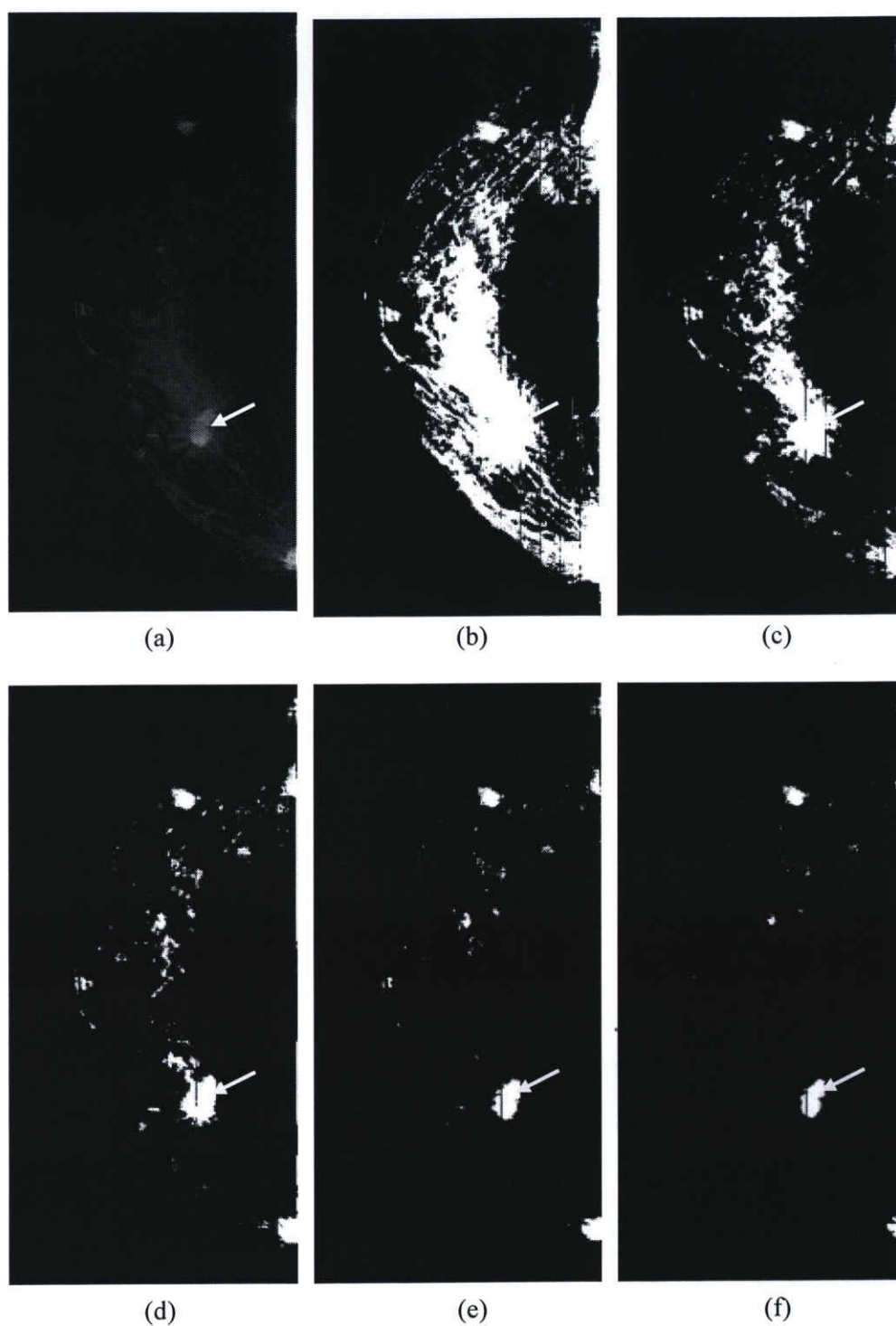
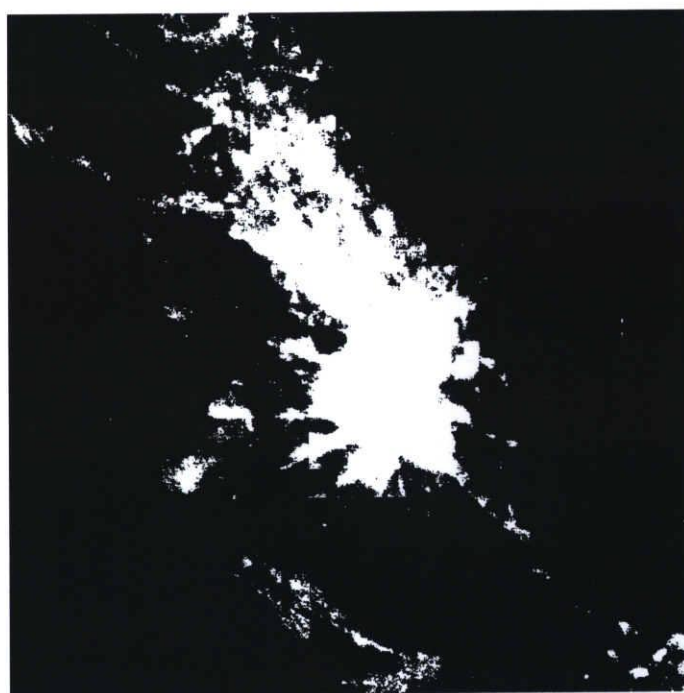


Figure 17 Segmented regions of potential mass based on different  $k$ : (a) subtraction image, (b) segmented regions of mass based on  $k = 0.0$ , (c) those based on  $k = 1.0$ , (d) those based on  $k = 2.0$ , (e) those based on  $k = 3.0$ , (f) those based on  $k = 4.0$ . Each arrow indicates the true mass region.





(a) Subtraction image in the small region



(b) Area with high pixel values segmented by the threshold pixel value for the center pixel of the small region.

Figure 18 Example of the segmentation of the area with high pixel values in the small region.

### 3.7. Detection of Mass

In candidates for mass, there are many candidates which are too larger or smaller than masses included in my database. It is obvious that they are not true mass. Therefore, only the candidates for mass with an appropriate size are detected as mass. Since masses included in my database had the diameters of 92 pixels to 1,150 pixels (approximately 4 mm to 50 mm), the appropriate size is defined as 4 mm to 50 mm. In the detection of mass, each of the candidates for mass is first surrounded by the rectangle, as shown in Figure 19. When the width and the height of the rectangle satisfy the appropriate size, its candidate is detected as mass. An example of result of detecting mass is shown in Figure 20.

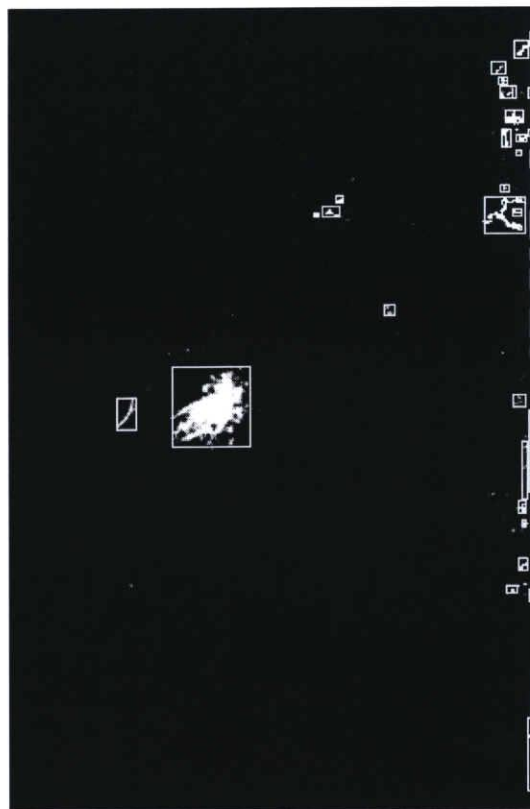
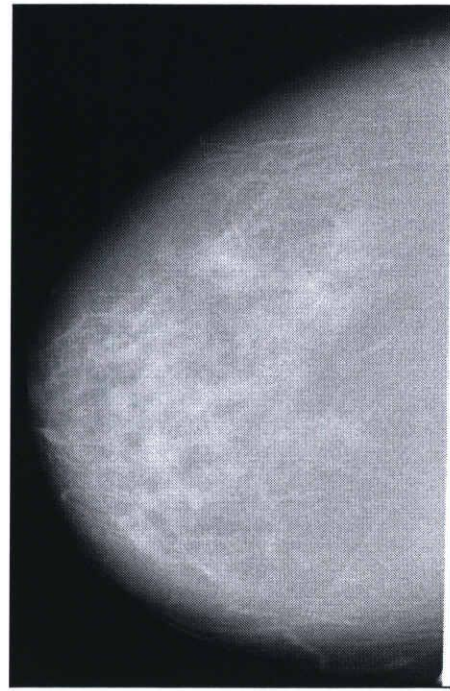


Figure 19 Example of candidates for mass with the circumscribed rectangle



(a) Right breast



(b) Left breast



(c) Detected candidates for mass

Figure 20 Example of the result of detecting mass: (a) original image of right breast, (b) original image of left breast, (c) detected candidates for mass on right breast. Each arrow indicates true mass region.

## 4. Results

It is necessary to determine the best parameters in the segmentation of candidates for mass. One of these parameters is the threshold value  $d$  about the difference of the mean values in each of white area and black area in the analysis of segmented pixel. Another is the parameter  $k$  of Niblack's thresholding technique.

Figure 21 shows the relationships between true-positive fraction and the mean number of false-positives per image when the threshold value  $d$  is varied from 50 to 5,000. When the center of the detected region as mass is within a true mass region, this region is considered to have been "truly" detected. When the center of the detected region as mass is not within a true mass region, this region is considered a false-positive. The true-positive fraction and the mean number of false-positives reduced as the threshold value  $d$  rose. However, using threshold value  $d$  of 150 was able to reduce about one false-positive per image without the reduction of true-positive fraction. Therefore, 150 was selected as the best threshold value about the difference of the mean values of pixel values in each of white area and black area in analysis of segmented pixel.

Figure 22 shows the relationships between true-positive fraction and the mean number of false-positives per image when the parameter  $k$  was varied from 0.0 to 5.0. The true-positive fraction and the mean number of false-positives reduced as the parameter  $k$  rose. This tendency appeared to be similar to that in Figure 21. The highest true-positive fraction was obtained when  $k$  was 2.0. Figure 23 shows the Free-response Receiver Operating Characteristic (FROC) curve [27] obtained by varying the parameter  $k$  while fixing the threshold value  $d$  at 150. Table 1 also shows the true-positive fractions and the mean numbers of false-positives when the parameter  $k$  had the three highest true-positive fractions. With the threshold value  $d$  of 150 and the parameter  $k$  of 2.0, the true-positive fraction and the mean numbers of false-positives were 93.4% (239/256) and 22.2/image (5683/256), respectively.

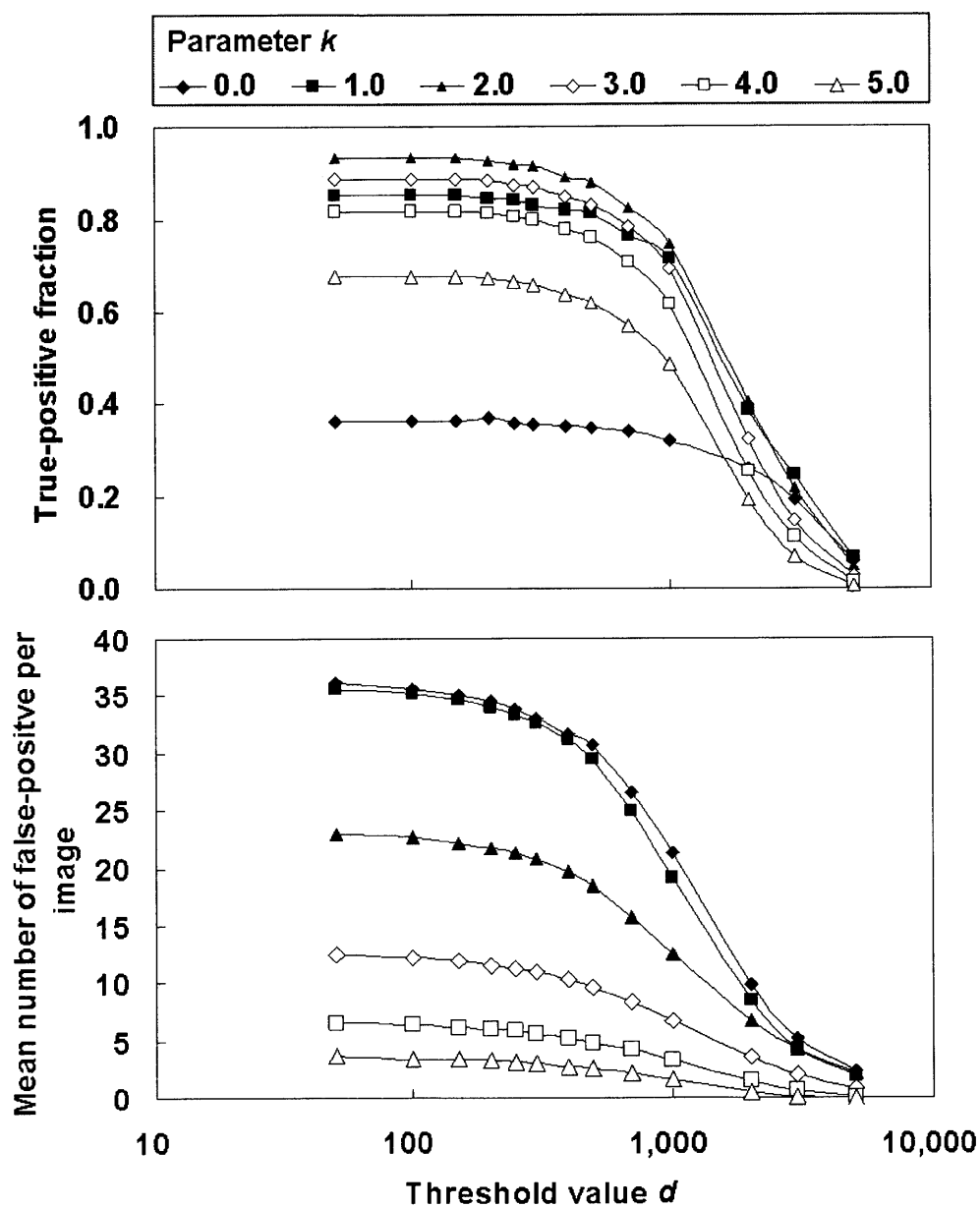


Figure 21 Relationships between true-positive fraction and the mean number of false-positives per image when the threshold value of  $d$  was varied from 50 to 5,000.

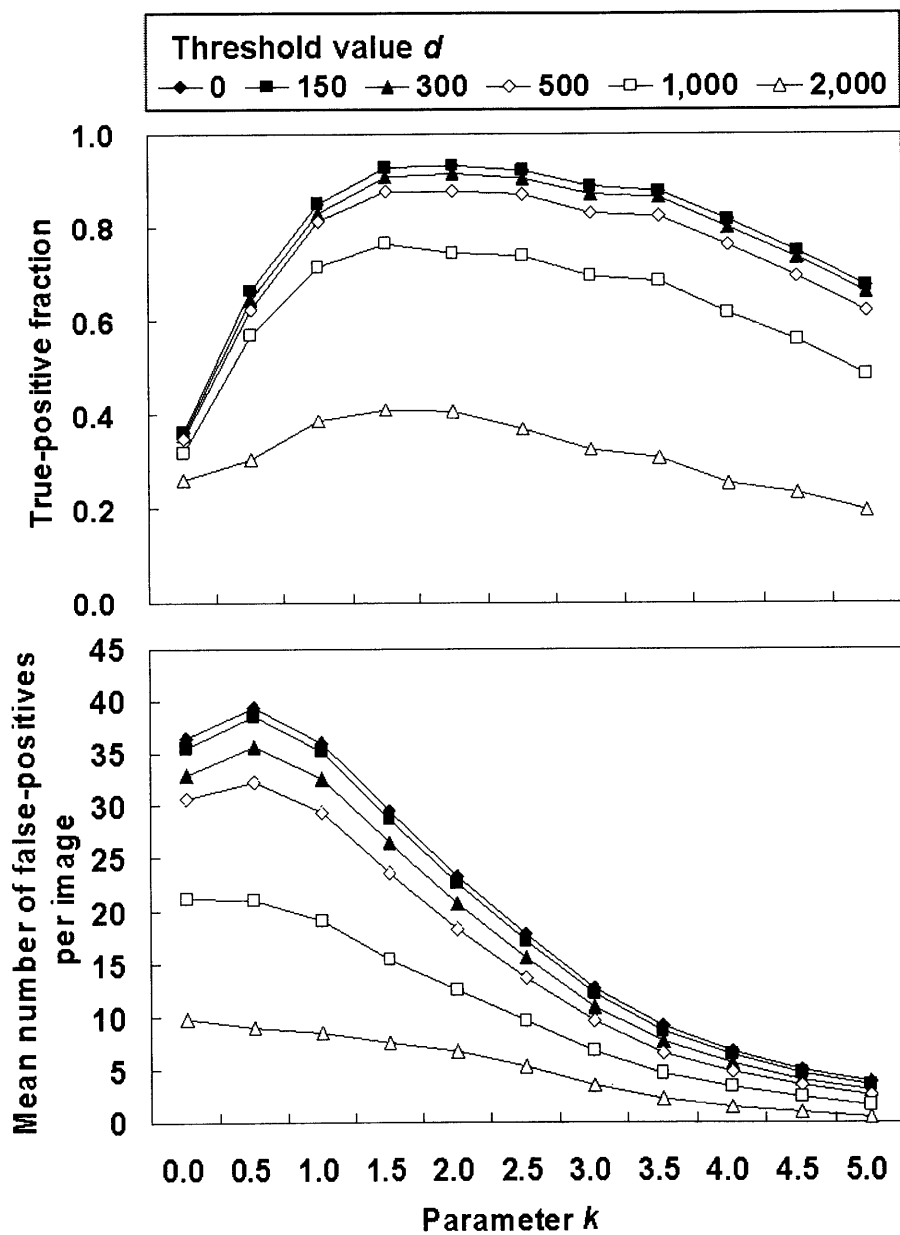


Figure 22 Relationships between true-positive fraction and the mean number of false-positives per image when the parameter  $k$  was varied from 0.0 to 5.0.

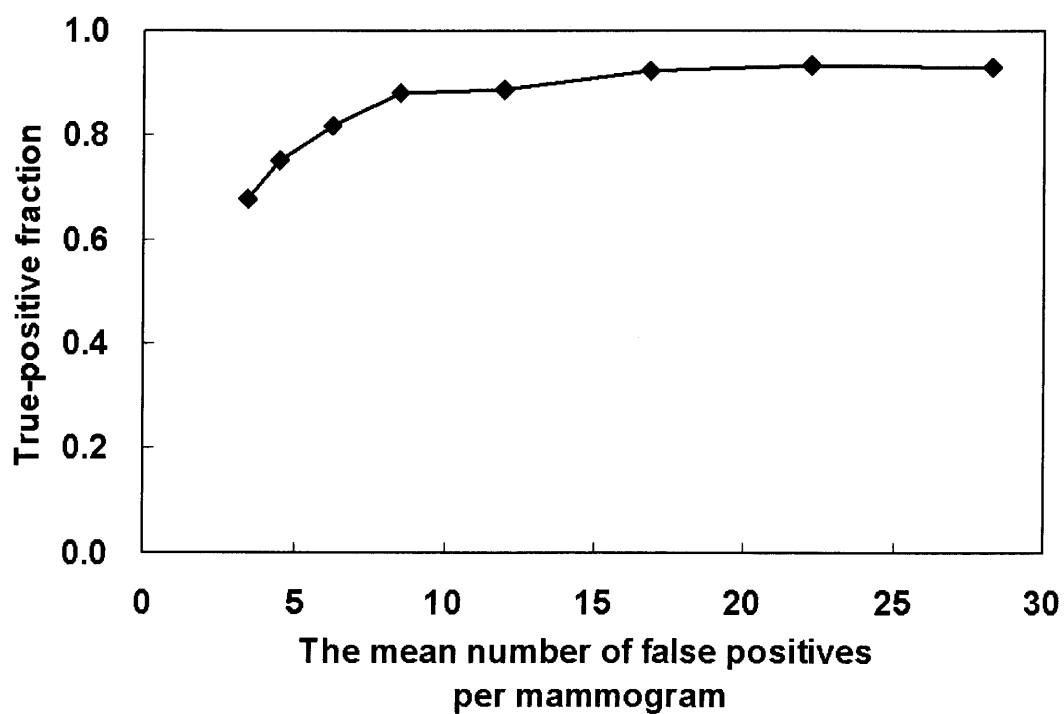


Figure 23 FROC curve obtained by varying the parameter  $k$  while fixing the threshold value  $d$  at 150

Table 1 Three highest true-positive fraction and the mean number of false-positives per image when the threshold value  $d$  was 150.

$k$	True-positive fraction	Mean number of false-positives per image
1.5	0.930	28.2
2.0	0.934	22.2
2.5	0.921	16.9

## ***5. Discussion***

### ***5.1. Comparison of Detection Performances***

In order to evaluate the usefulness of proposed CAD scheme, the detection performance of proposed CAD scheme was compared with other three computerized schemes for detection of masses. Proposed CAD scheme consisted of the enhancement of nodular structures, the alignment of right and left breast regions based on skin lines, the alignment of right and left breast regions based on similar ROIs, and the segmentation of candidates for mass whereas computerized scheme 1 corresponding to a conventional method consisted of the alignment of right and left breast regions based on skin lines and the segmentation of candidates for mass. Computerized scheme 2 consisted of the alignment of right and left breast regions based on skin lines, the alignment of right and left breast regions based on similar ROIs, and the segmentation of candidates for mass. Computerized scheme 3 also consisted of the enhancement of nodular structures, the alignment of right and left breast regions based on skin lines, and the segmentation of candidates for mass. Table 2 shows the conditions of proposed CAD scheme and other three computerized schemes. Figure 24 shows the FROC curves of proposed CAD scheme and other three computerized schemes. The detection performances of computerized scheme 2 and computerized scheme 3 were much higher than that of computerized scheme 1. This result indicated the usefulness of the alignment of right and left breast regions based on similar ROIs and the enhancement of nodular structures, which were not used in a conventional method. The detection performance of a conventional method (computerized scheme 1) was substantially improved by adding the enhancement of nodular structures and the alignment of right and left breast regions based on similar ROIs. The detection performance of proposed CAD scheme tended to be higher than that of other computerized schemes.



Table 2 Condition of proposed CAD scheme and other three computerized schemes

	(a) Alignment based on skin lines	(b) Alignment based on similar ROIs	(c) Enhancement of nodular structures
Computerized Scheme 1 (Conventional method)	○	—	—
Computerized scheme 2 (Conventional method + (b))	○	○	—
Computerized scheme 3 (Conventional method + (c))	○	—	○
Proposed CAD scheme	○	○	○

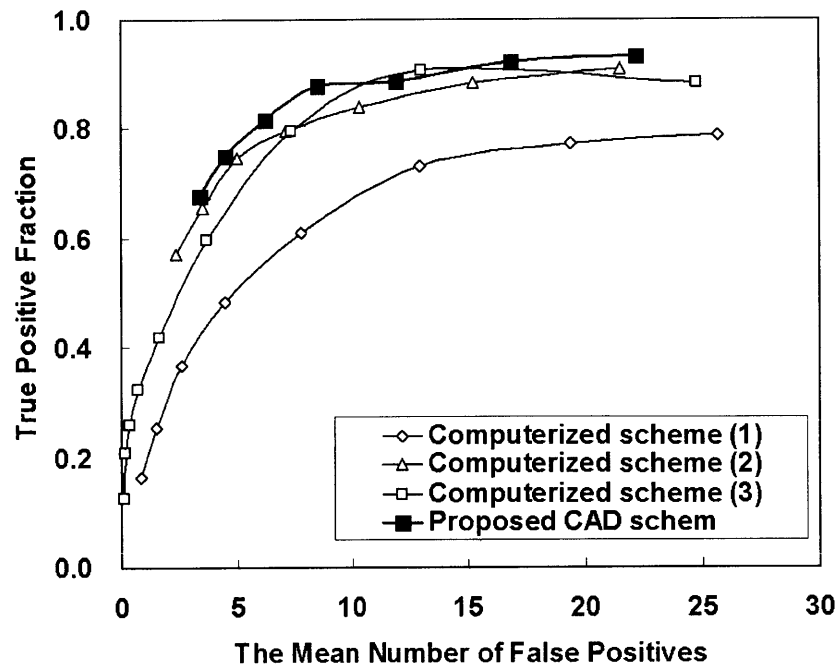
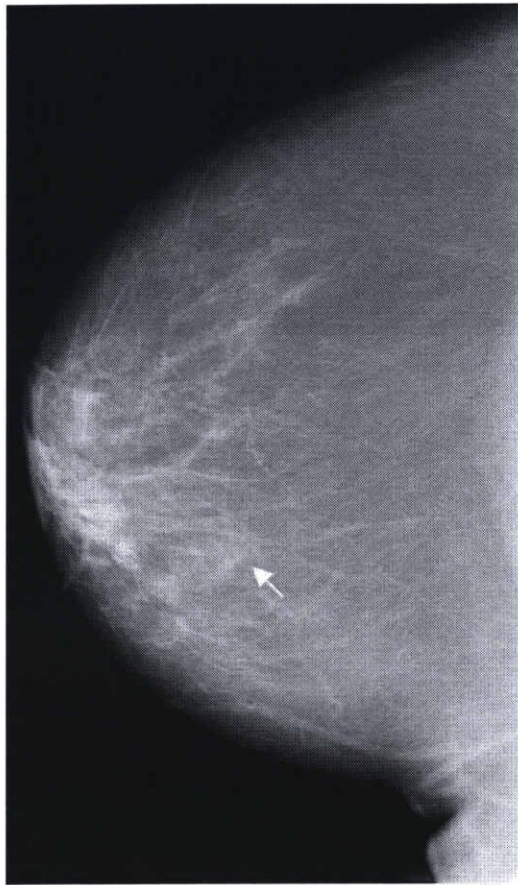


Figure 24 FROC curves obtained by varying parameter  $k$  while fixing the threshold value  $d$  at 150

## ***5.2. Undetected masses***

There were common features in masses which were not detected by proposed CAD scheme. These image features were: (1) the contrast between mass region and the surrounding normal tissues was very low; (2) the margin of mass was very blurred. Figure 25 shows an example of original mass with undetected mass and the enhanced image for nodular structures. In the case of Figure 25, the nodular structures except mass region were enhanced greatly whereas mass region wasn't enhanced effectively. Therefore, it is necessary to improve a scheme for enhancing nodular structures in order to detect very obscure masses.

As the case of undetected mass, there were cases which have large difference in skin lines between right and left breast regions. Figure 26 shows an example of which right and left breasts which were not aligned correctly because of large difference in skin lines. The large difference in skin lines between right and left breasts caused a failure in the alignment of right and left breast regions based on skin lines. Therefore, it was impossible to align right and left breast regions more accurately based on similar ROIs correctly. In order to align right and left breast regions based on similar ROIs effectively, it is important to align right and left breast regions based on skin lines. The true-positive fraction might be improved by employing more robust alignment of right and left breast regions.



(a) Original image

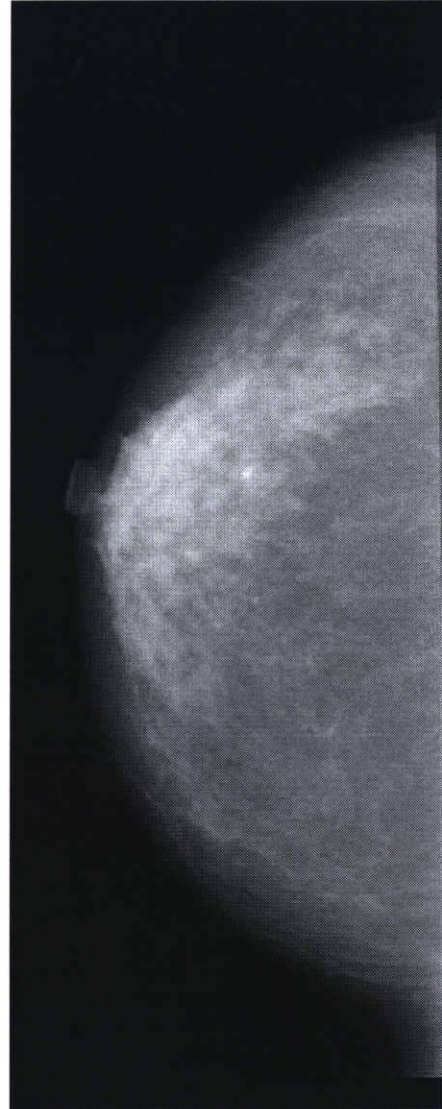


(a) Enhanced image for nodular structures

Figure 25 Example of original image with undetected mass and the enhanced image for nodular structures. Each arrow indicates the true mass region.



(a) Left breast



(b) Right breast

Figure 26 Example of right and left breasts which were not aligned correctly because of large difference in skin lines. The arrow indicates the true mass region.



## ***6. Development of Graphical User Interface for Proposed CAD Scheme***

### ***6.1. Overview of Graphical User Interface***

In order to use proposed CAD scheme in screening mammograms, the GUI (Graphical User Interface) for proposed CAD scheme was developed with Microsoft Visual C# 2005 on Windows XP. Figure 27 shows the screenshot of the GUI.

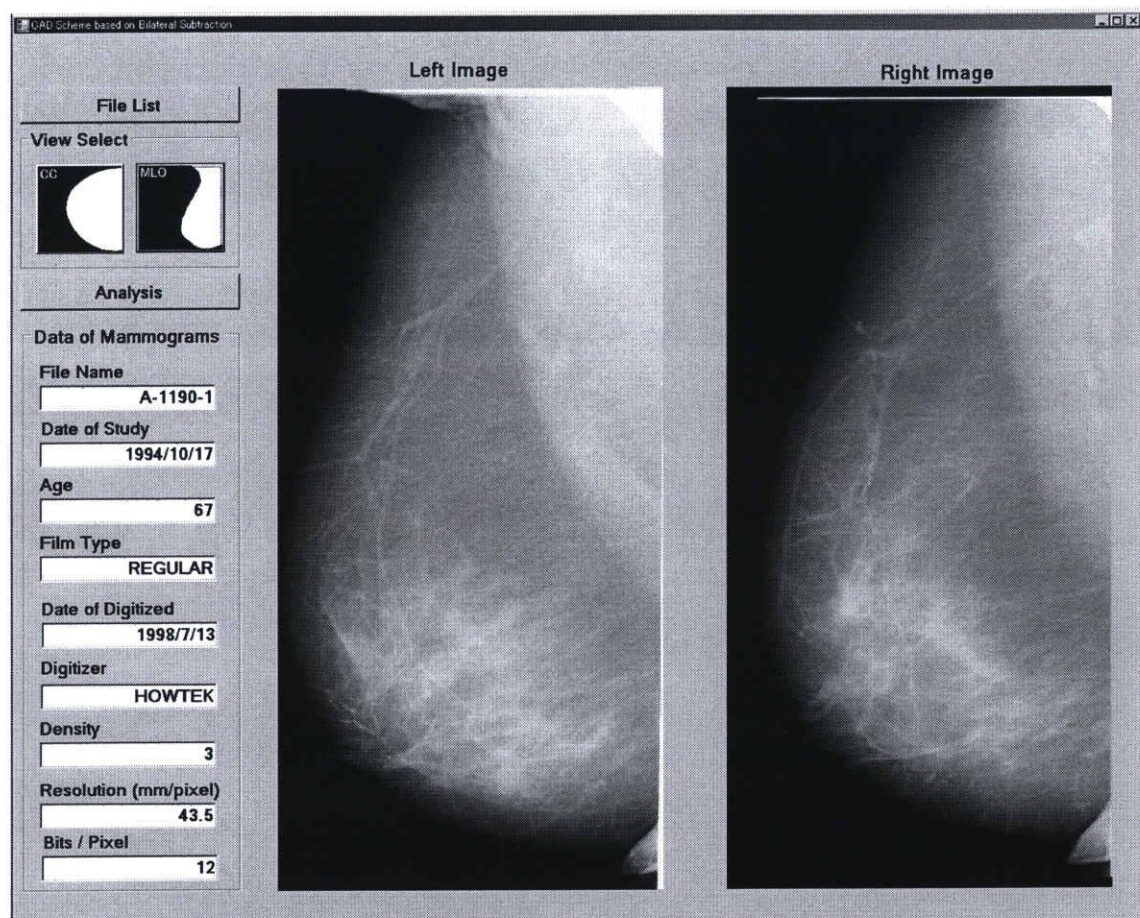


Figure 27 Screenshot of GUI for proposed CAD scheme

## ***6.2. Display of Breast Images and the Analysis Result of proposed CAD Scheme***

This GUI displays a pair of right and left breast (right side of Figure 27) and the patient information (left side of Figure 27) when a mammogram is selected from file list. This GUI also displays the analysis result of proposed CAD scheme for detection of masses when the analysis button is clicked. In addition, the enlargement of image, the brightness of image, and the contrast of image are able to be transformed by mouse operations. The mouse operations for these transformations are as follows:

### **Image enlargement / reduction**

A left-mouse clicking with the selecting the enlargement button will show you the enlarged image. There are five possible enlargement levels: 1.0, 2.0, 3.0, 4.0, and 5.0. The enlarged image will be zoomed out by a left-mouse clicking with selecting the reduction button.

### **Brightness transform**

A right-mouse dragging to a horizontal direction will transform the brightness of the image. If the mouse is moved leftward, the brightness of the image will be getting dark. On the other hand, if the mouse is moved rightward, the brightness of the image will be getting bright.

### **Contrast transform**

A right-mouse dragging to a vertical direction will transform the contrast of the image. If the mouse is moved upward, the contrast of the image will be getting high. On the other hand, if the mouse is moved to downward, the contrast of the image will be getting low.

## ***7. Conclusion***

In this paper, I developed a new CAD scheme for detection of masses based on bilateral subtraction techniques using the alignment of right and left breast regions based on normal structures. The detection performance of proposed CAD scheme was evaluated by using 512 mammograms selected randomly from DDSM. Proposed CAD scheme achieved the sensitivity of 93.4% (239/256) at 22.2 (5683/256) false-positives per image, while the sensitivity of the conventional method was 78.9% (202/256) at 25.7 (6579/256) false-positives per image. This result indicates that proposed CAD scheme improved the detection performance of mass.

Nevertheless, some important ideas remain to increase the sensitivity. As I described in the chapter 5, some very obscure masses were not enhanced effectively. Therefore, it is necessary to improve the scheme for enhancing nodular structures in order to increase the sensitivity. In addition, many false-positives were detected with the true mass in proposed CAD scheme. The many false-positives make radiologists' interpretation difficult. Therefore, it is also necessary to reduce false-positives without reduction of sensitivity.

## ***Acknowledgment***

I'm grateful to Prof. Shinji Tsuruoka, Prof. Tsuyoshi Shinogi and Assistant Prof. Hiroharu Kawanaka for useful advice and to Assistant Prof. Ryohei Nakayama of School of Medicine, Mie University for teaching and discussions. Many thanks are due to the members of Information Processing Laboratory in School of Engineering, Mie University.



## Appendix: Histogram Specification

$p_k(i)$  which is the probability of an occurrence of pixel value  $i$  on the breast  $k$  (right and left) and  $C_k(i)$  which is the cumulative distribution function corresponding to  $p_k(i)$  are defined by

$$\text{probability of an occurrence of pixel value: } p_k(i) = \frac{n_i}{n_k}, i \in 0, \dots, 4095 \quad (7)$$

$$\text{cumulative distribution function: } C_k(i) = \sum_{j=0}^i p_k(j) \quad (8)$$

Here,  $n_i$ ,  $n_k$ , and 4095 are the frequency of pixel value  $i$ , the total number of pixel on a breast region  $k$ , respectively.  $y_{left}$  is then regarded as  $C_{left}(i'_{left})$  which is the value of cumulative distribution function on pixel value  $i'_{left}$ . Moreover, a transform is defined by

$$y_{left} = T(i'_{left}) \quad (9)$$

The inverse of the above transformations are

$$\begin{aligned} i'_{left} &= T^{-1}(y_{left}) \\ &= T^{-1}(C_{left}(i'_{left})) \end{aligned} \quad (10)$$

In the histogram specification,  $i'_{right}$  is corresponded to  $i'_{left}$  which has the same cumulative frequency as  $C_{right}(i'_{right})$ . Therefore,  $i'_{right}$  and  $i'_{left}$  must satisfy the condition

$$C_{right}(i'_{right}) = C_{left}(i'_{left}) \quad (11)$$

Therefore, the transform from  $i'_{right}$  to  $i'_{left}$  is expressed by

$$i'_{left} = T^{-1}(C_{right}(i'_{right})) \quad (12)$$

The histograms based on pixel values are uniformed between the right and left breasts by employing this transform to all pixel values in the right breast region.

## ***References***

- [1] American Cancer Society, “Cancer Facts and Figures 2007”, 2007
- [2] Ministry of Health, Labor and Welfare, “Population Survey Report” (in Japanese), 2006
- [3] R. E. Bird, T. W. Wallace, and B. C. Ynakaskas, “Analysis of cancers missed at screening mammography”, *Radiology*, Vol.184, pp.613-617, 1997
- [4] K. Doi, H. MacMahon, S. Katsuragawa, R. M. Nishikawa, and Y. Jiang, “Computer-aided diagnosis in radiology: potential and pitfalls”, *European Journal of Radiology*, Vol.31, No.2, pp.97-109, 1997
- [5] R. Nakayama “Toward practical application and spread of CAD for mammography”, *GE today*, GE Healthcare, Vol.23, pp.51-52, 2007
- [6] L. J. W. Burhenne, S. A. Wood, C. J. D'Orsi, S. A. Feig, D. B. Kopans, K. F. O'Shaughnessy, E. A. Sickles, L. Tabar, C. J. Vyborny, and R. A. Castellino, “Potential Contribution of Computer-aided Detection to the Sensitivity of Screening Mammography”, *Radiology*, Vol.215, pp.554-562, 2000
- [7] T. W. Freer and M. J. Ulissey, “Screening Mammography with Computer-aided Detection: Prospective Study of 12,860 Patients in a Community Breast Center”, *Radiology*, Vol.220, pp.781-786, 2001
- [8] M. A. Kupinski and M. L. Giger, “Automated Seeded Lesion Segmentation on Digital Mammograms”, *IEEE Transaction on Medical Imaging*, Vol.17, Issue 4, pp.510-517, 1998
- [9] N. Petrick, H. P. Chan, B. Sahiner, and D. Wei, “An Adaptive Density-Weighted Contrast Enhancement Filter for Mammographic for Mammographic Breast Mass Detection”, *IEEE Transactions on Medical Imaging*, Vol.15, Issue 1, pp.59-67, 1996
- [10] N. Petrick, H. P. Chan, D. Wei, B. Sahiner, M. A. Helvie, and D.D. Adler, “Automated Detection of Breast Masses on Mammograms using Adaptive Contrast Enhancement and Texture Classification”, *Medical Physics*, Vol.23, Issue 10, pp.1685-1696, 1996
- [11] N. Karssemeijer, and G. M. te Brake, “Detection of stellate distortions in mammograms”, *IEEE Transactions on Medical Imaging*, Vol.15, Issue 5, pp.611-619, 1996

- [12] T. Matsubara, H. Fujita, T. Endo, K. Horikita, M. Ikeda, C. Kido, and T. Ishigaki, "Development of a High-speed Processing Algorithm for Mass Detection Based on Thresholding Technique in Mammograms" (in Japanese), *Medical Imaging Technology*, Vol.15, No.1, pp.1-13, 1997
- [13] H. Kobatake and M. Murakami, "Adaptive Filter to Detect Rounded Convex Regions : Iris Filter", *Proc. of International Conference on Pattern Recognition (ICPR)*, 1996
- [14] A. Shimizu, J. Hasegawa, and J. Toriwaki, "Characteristics of Rotatory Second Order Difference Filter for Computer Aided Diagnosis of Medical Images" (in Japanese), *IEICE Transactions*, Vol. J76-D-II, No.2, pp.29-39, 1993
- [15] S. Yamamoto, "Characteristics of Quoit Filter, a Digital Filter Developed for the Extraction Circumscribed Shadows, and Its Applications to X-ray CT Images" (in Japanese), *Medical Imaging Technology*, Vol.12, No.1, pp.67-73, 1994
- [16] D. Kopans, "Breast Imaging", Lippincott-Raven, Philadelphia, 1998
- [17] F. F. Yin, M. L. Giger, K. Doi, H. Yoshimura, X. W. Xu, J. Balter, and CE Meltz, "Automated registration of digital mammograms for use in mammographic computer vision schemes", *Medical Physics*, Vol.18, pp.524, 1990
- [18] N. Karssemeijer, and G. M. te Brake, "Combining Single View Features and Asymmetry for Detection of Mass Lesions", *Digital mammography*, Nijmegen, pp.935-102, 1998
- [19] DDSM (Digital Database for Screening Mammography, University of South Florida), <http://marathon.csee.usf.edu/Mammography/Database.html>
- [20] M. Heath, K. Bowyer, D. Kopans, R. Moore and W. Philip Kegelmeyer, "The Digital Database for Screening Mammography", *Proceedings of the Fifth International Workshop on Digital Mammography*, Medical Physics Publishing, pp.212-218, 2001
- [21] M. Heath, K. Bowyer, D. Kopans, W. P. Kegelmeyer, R. Moore, K. Chang, and S. MunishKumaran, "Current Status of the Digital Database for Screening Mammography", *Digital Mammography*, *Proc. of the Fourth International Workshop on Digital Mammography*, pp.457-460, 1998
- [22] R. C. Gonzalez and R. E. Woods, "Digital Image Processing" , MA: Addison-Wesley, 1992

- [23] J. Serra, "Image Analysis and Mathematical Morphology", Academic Press, London, 1982
- [24] R Nakayama, Y Uchiyama, K Yamamoto, R Watanabe, and K Namba, "Computer-Aided Diagnosis Scheme using a Filter Bank for Detection of Micro Calcification Clusters in Mammograms", IEEE Transactions on Biomedical Engineering, Vol.53, No.2, pp.273-283, 2006
- [25] E. R. Davis, "Machine Vision Theory, Algorithms, Practicalities third edition", Morgan Kaufmann Publishers, pp.196-197, 2005
- [26] W. Niblack, "An Introduction to Digital Image Processing", Prentice Hall, 1985
- [27] D. P. Chakraborty and L. H. L. Winter, "Free-response methodology: alternate analysis and a new observer- performance experiment", Radiology, Vol.174, pp.873-881, 1990

## ***Research Accomplishment***

### 学術論文

- (1) 水谷洋輔, 鶴岡信治, 川中普晴, 篠木剛, 大山航, 関岡清次, “超音波RF信号からの局所心筋の運動追跡による心筋を対象とした運動機能評価指標”, 日本知能情報ファジィ学会誌, Vol. 20, pp.19-28, February, 2008

### 国際会議

- (1) Yosuke Mizutani, Shinji Tsuruoka, Hiroharu Kawanaka, Tsuyoshi Shinogi, Wataru Ohyama, and Kiyotugu Sekioka, “New Indexes on Heart Motion Evaluation Using Ultrasonic RF Signal”, Proceeding of Joint 3rd International Conference on Soft Computing and Intelligent Systems and 7th International Symposium on Advanced Intelligent Systems, pp.2001-2006, 2006
- (2) Yosuke Mizutani, Shinji Tsuruoka, Hiroharu Kawanaka, Tsuyoshi Shinogi, Wataru Ohyama, and Kiyotugu Sekioka, “Heart Motion Evaluation Indexes Using Ultrasonic RF signal”, Proceeding of International Conference on Hybrid Information Technology, Vol.2, pp.62-67, 2006

### 国内会議

- (1) 水谷洋輔, 中山良平, 竹田寛, 川中普晴, 高田孝広, 山本皓二, 鶴岡信治, “左右乳房の比較に基づいた腫瘍陰影検出支援システムの開発”, 第 27 回医療情報学連合大会 (第 8 回日本医療情報学会学術大会) 論文集, pp.1048-1049
- (2) 中山良平, 渡辺良二, 水谷洋輔, 高田孝広, 山本皓司, 竹田寛, “乳房 X 線写真における構築の乱れ検出支援システムの開発”, 第 27 回医療情報学連合大会 (第 8 回日本医療情報学会学術大会) 論文集, pp.1046-1047

### 受賞等

- (1) “Session Best Presentation Award”, Joint 3rd International Conference on Soft Computing and Intelligent Systems and 7th International Symposium on Advanced Intelligent Systems